

1 **EnKF assimilation of high-resolution, mobile Doppler radar data of the 4 May 2007**  
2 **Greensburg, Kansas supercell into a numerical cloud model**

3  
4 Robin L. Tanamachi<sup>1, 2, 3</sup>

5 Louis J. Wicker<sup>4</sup>

6 David C. Dowell<sup>5</sup>

7 Howard B. Bluestein<sup>3</sup>

8 Daniel T. Dawson II<sup>2, 4</sup>

9 Ming Xue<sup>1</sup>

10  
11 <sup>1</sup>*Center for Analysis and Prediction of Storms, University of Oklahoma, Norman, Oklahoma*

12 <sup>2</sup>*Cooperative Institute for Mesoscale Meteorological Studies, Norman, Oklahoma*

13 <sup>3</sup>*School of Meteorology, University of Oklahoma, Norman, Oklahoma*

14 <sup>4</sup>*National Severe Storms Laboratory, Norman, Oklahoma*

15 <sup>5</sup>*NOAA Earth Systems Research Laboratory, Boulder, Colorado*

16  
17 Revised submission to:

18 *Monthly Weather Review*

19 10 July 2012

20  
21 Corresponding author address:

22 Robin L. Tanamachi

23 Center for Analysis and Prediction of Storms

24 University of Oklahoma

25 120 David L. Boren Blvd., Suite 2500

26 Norman, OK 73072

27 rtanamachi@ou.edu

1 **Abstract**

2 Mobile Doppler radar data, along with observations from a nearby WSR-88D, are assimilated  
3 with an ensemble Kalman filter (EnKF) technique into a non-hydrostatic, compressible  
4 numerical weather prediction model to analyze the evolution of the 4 May 2007 Greensburg,  
5 Kansas tornadic supercell. The storm is simulated via assimilation of reflectivity and velocity  
6 data in an initially horizontally homogeneous environment whose parameters are believed to be a  
7 close approximation to those of the Greensburg supercell inflow sector. Experiments are  
8 conducted to test analysis sensitivity to mobile radar data availability and to the mean  
9 environmental near-surface wind profile, which was changing rapidly during the simulation  
10 period. In all experiments, a supercell with similar location and evolution to the observed storm  
11 is analyzed, but the simulated storm's characteristics differ markedly. The assimilation of mobile  
12 Doppler radar data has a much greater impact on the resulting analyses, particularly at low  
13 altitudes ( $\leq 2$  km), than modifications to the near-surface environmental wind profile.  
14 Differences in the analyzed updrafts, vortices, cold pool structure, rear-flank gust front structure,  
15 and observation-space diagnostics are documented. An analyzed vortex corresponding to the EF-  
16 5 Greensburg tornado is stronger and deeper in experiments in which mobile (higher resolution)  
17 Doppler radar data are included in the assimilation. This difference is linked to stronger analyzed  
18 horizontal convergence, which in turn is associated with increased stretching of vertical vorticity.  
19 Changing the near-surface wind profile appears to impact primarily the updraft strength,  
20 availability of streamwise vorticity for tilting into the vertical, and low-level vortex strength and  
21 longevity.

22

# 1 **1. Introduction**

2 Radar is one of few atmospheric measurement tools capable of collecting volumetric data  
3 resolving sub-storm scale features. Assimilation of radar data into numerical weather prediction  
4 (NWP) models to improve understanding of convective storm dynamics is now a fairly routine  
5 exercise, and analysis and prediction of high-impact, sub-storm scale features such as tornadoes  
6 is a natural objective. Numerous studies have been undertaken in this area in the past two  
7 decades; summaries of these efforts are provided by Lilly (1990), Sun (2005), Kain et al. (2010),  
8 and Stensrud et al. (2009).

9 Weather Surveillance Radar-1988 Doppler (WSR-88D) data are now routinely collected  
10 across most of the contiguous United States. The two measured radar variables most often  
11 assimilated into NWP models are Doppler velocity ( $V_r$ ) and radar reflectivity factor ( $Z$ ). NWP  
12 models require and calculate additional state variables (e.g., temperature and pressure) that  
13 observations of  $V_r$  and  $Z$  do not furnish. While a Doppler radar can provide detailed velocity  
14 information within convective storms, the cross-beam components of velocity are unobserved  
15 and must be calculated or inferred. The quantity  $Z$  is integrated over many different  
16 hydrometeors with variable scattering properties (Doviak and Zrnić 1993), and has nonlinear  
17 relationships with model state variables related to hydrometeors (Snyder and Zhang 2003;  
18 Dowell et al. 2011). The ensemble Kalman filter (EnKF) (Evensen 1994; Houtekamer and  
19 Mitchell 1998) provides an attractive pathway toward inferring unobserved model state variables  
20 based, at least in part, on Doppler radar measurements (Snyder and Zhang 2003; Dowell et al.  
21 2004a; Dowell et al. 2004b; French et al. 2006; Jung et al. 2008a; Aksoy et al. 2009; Dowell and  
22 Wicker 2009; Dowell et al. 2011; Snook et al. 2011).

1 Owing to the scanning geometry and wide geographic spacing of the WSR-88D (more than  
2  $200^2$  km<sup>2</sup>), substantial regions of the atmosphere remain unobserved at altitudes below 1 km  
3 AGL, where weather events directly impact human activity (National Research Council 1995).  
4 Zhang et al. (2004) found that assimilation of radial velocity observations at and below 2 km  
5 AGL improved analyzed cold pool structure. Snook et al. (2011) demonstrated that assimilation  
6 of  $Z$  and  $V_r$  data from short-range, stationary, X-band Collaborative Adaptive Sensing of the  
7 Atmosphere (CASA) radars, in addition to data from a WSR-88D, greatly impacted analyzed  
8 low-level wind fields in a 2007 tornadic mesoscale convective system. In particular, the analyzed  
9 locations of near-surface wind features such as gust fronts and miso-vortices were improved via  
10 assimilation of shallow volumes of CASA data. Previous studies have indicated that the locations  
11 of such near-surface features may be crucial to tornadogenesis (Marquis et al. 2008; Wurman et  
12 al. 2010; Markowski et al. 2011b; Marquis et al. 2012).

13 In this study, we assimilate  $V_r$  data from an X-band, mobile Doppler radar in addition to  
14 WSR-88D  $Z$  and  $V_r$  data into the National Severe Storms Laboratory (NSSL) Collaborative  
15 Model for Multiscale Atmospheric Simulation (NCOMMAS; Wicker and Skamarock 2002;  
16 Coniglio et al. 2006), and assess the impact on storm-scale EnKF analyses of the 4 May 2007  
17 Greensburg, Kansas tornadic supercell (hereafter “the Greensburg storm”). This historic storm  
18 produced at least 22 tornadoes over a period of 9 hrs, including an EF-5 tornado that devastated  
19 the town of Greensburg, Kansas at 0245-0250 UTC (Lemon and Umscheid 2008; Bluestein  
20 2009), causing 11 fatalities. The University of Massachusetts mobile, X-band, polarimetric  
21 Doppler radar (UMass X-Pol; Bluestein et al. 2007) captured much of the Greensburg storm’s  
22 early evolution, collecting data in at least ten tornadoes (Tanamachi et al. 2012). Since the  
23 UMass X-Pol was located closer to the hook echo of the Greensburg storm and collected data at

1 lower levels than the nearest WSR-88D, this data set provides an unusual opportunity to examine  
2 the impacts of assimilating mobile Doppler radar data on EnKF analyses of a supercell.

3 Mobile Doppler radar can potentially move close to a target storm and sample an area of  
4 interest near the surface. While data from mobile X-band Doppler radars have been assimilated  
5 via EnKF into NWP models in previous studies (French 2006; Marquis et al. 2010; Marquis et al.  
6 2012), only one other study is known to the authors in which data from a mobile Doppler radar  
7 and WSR-88D data were assimilated together (Marquis et al. 2010). In that study, as in this one,  
8 radar data were assimilated into an initially horizontally homogeneous environment with a flat  
9 model bottom boundary. The Greensburg storm occurred over rather flat terrain (southwest  
10 Kansas), so we consider our use of a flat model bottom boundary reasonable.

11 The locations of stationary radars and their orientation in space are generally well-  
12 documented. Such radars are sited on tall platforms to minimize beam blockage, and clutter  
13 patterns around the radars become known to the data users with time. In contrast, assimilation of  
14 data from mobile Doppler radars poses additional challenges. The mobile radar may be deployed  
15 under challenging conditions (e.g., in great haste, on uneven surfaces, or in severe weather), and  
16 its orientation may not be well documented. This issue has been mitigated to some extent  
17 through the use of Global Positioning System (GPS) devices, which can record the radar location  
18 to within 10 m, and hydraulic leveling systems, which can ensure a level antenna base to within  
19  $\pm 0.2^\circ$ . In addition, because the radar antenna is height-constrained for transportability, the  
20 transmitted radar signal is more susceptible to blockage by trees, hills, buildings, and telephone  
21 poles. Ground clutter patterns around the radar change with every deployment. The clutter  
22 around the antenna may be documented via photographs, site surveys, maps, and/or the radar

1 data. Usually, as in this case, extensive quality control must be applied to mobile Doppler radar  
2 data before they can be assimilated into an NWP model.

3 Our study also addresses the relative impact on analyses of modification of an initial  
4 boundary layer wind profile. Bluestein (2009) speculated that an intensifying low-level jet in the  
5 Greensburg storm’s environment may have played a role in the formation and intensification of  
6 the Greensburg tornado. Do changes to the wind profile impact the analyzed storms and  
7 accompanying vortices? For how long does the model “remember” an initial wind profile, once  
8 radar data are assimilated? These questions were partially addressed in a companion study  
9 (Dawson et al. 2012) that focused on the impact of modifications to the boundary layer wind  
10 profile on *forecasts* of the Greensburg storm and its vortices. In this study, we focus on how  
11 changes to the boundary layer wind profile impact the analyses.

12 We briefly summarize the meteorological background of the Greensburg storm and the radar  
13 data used in this study in the next section (2). Section 3 details our NCOMMAS experiments,  
14 including the development of the initial model environment, experiment parameters, radar data  
15 quality control and objective analysis. Experiment results, which show substantial impacts from  
16 both mobile radar data assimilation and modification of the initial wind profile, are presented in  
17 Section 4. Section 5 summarizes the study.

## 18 **2. The 4 May 2007 Greensburg, Kansas storm and radar data**

19 Because the Greensburg storm has been well documented by Lemon and Umscheid (2008),  
20 Monfredo (2008), Bluestein (2009), and Tanamachi et al. (2012), only a brief review of its early  
21 evolution will be given here. The Greensburg storm formed at 0030 UTC on an outflow  
22 boundary from a previous storm, became a mature supercell over the next hour (Fig. 1), and

1 produced four EF-0 and EF-1 tornadoes (tornadoes 1-4) from 0132 to 0155 UTC (Fig. 2).  
2 Tornado 5 (“the Greensburg tornado”) formed at 0200 UTC, generated a 53 km-long damage  
3 path, inflicted EF-5 damage in Greensburg, Kansas from 0245 to 0250 UTC, and finally  
4 dissipated at 0305 UTC. The Greensburg tornado was accompanied by at least seven smaller,  
5 satellite tornadoes (6-12) from 0210 to 0259 UTC (Lemon and Umscheid 2008). Although this  
6 storm produced several additional significant tornadoes, we are primarily concerned with the  
7 time span (through 0300 UTC) covering the first 10 in the sequence (Tanamachi et al. 2012).

8 In this study, only radar data were assimilated, not only to limit the complications introduced  
9 by the addition of other data sources, but also because few supplemental data were available.  
10 (Those observations were used to specify the initial model environment, as described below.) We  
11 assimilated  $Z$  and  $V_r$  data from the WSR-88D in Dodge City, Kansas (KDDC) and, in some  
12 experiments,  $V_r$  data from the University of Massachusetts mobile, X-band, polarimetric Doppler  
13 radar (UMass X-Pol; Bluestein et al. 2007; Tanamachi et al. 2012). Some relevant characteristics  
14 of these two radars are shown in Table 1.

15 *a. WSR-88D data*

16 The Greensburg tornado occurred at a range of ~60 km from the WSR-88D at the National  
17 Weather Service (NWS) forecast office in Dodge City, Kansas (KDDC; Table 1; Fig. 3). KDDC  
18 collected data continuously at 4.1 minute intervals in the Greensburg storm, including its  
19 initiation at 0030 UTC<sup>1</sup>. In Volume Coverage Pattern 12 (VCP12; Brown et al. 2005), a WSR-  
20 88D executes a “step-spiral” scanning pattern, cycling through fourteen elevation angles ranging  
21 from 0.5° to 19.5°. We used 37 volumes of KDDC  $Z$  and  $V_r$  data, from 0029 to 0302 UTC.

---

<sup>1</sup> The Greensburg storm was also detected by KVNK and the WSR-88D located at the NWS forecast office in Amarillo, Texas (KAMA), among others. The distance between the Greensburg tornado and KVNK was ~130 km; for KAMA this distance was ~330 km.

1 Because the data exhibited velocity aliasing, they were manually dealiased using National Center  
2 for Atmospheric Research (NCAR) Solo II radar data editing and visualization software (Oye et  
3 al. 1995).

#### 4 *b. UMass X-Pol data*

5 As part of an ongoing severe weather research effort, UMass X-Pol (Bluestein et al. 2007)  
6 was deployed 48 km south-southwest of Greensburg, and collected data in the Greensburg storm  
7 continuously from 0112 to 0233 UTC (apart from one six-minute break when the truck had to be  
8 moved in order to minimize beam blockage to the west; Fig. 2). The UMass X-Pol azimuthal  
9 sector (around 90 degrees wide in most instances) was rotated clockwise toward the north to  
10 follow the target storm. Initially, the crew collected shallow volumes ( $3 - 10^\circ$ ), but switched to  
11 deeper volumes ( $3 - 15^\circ$  or  $3 - 20^\circ$ ) as tornado 5 matured. A complete description of the  
12 deployment can be found in Tanamachi et al. (2012).

### 13 **3. Experiment setup**

#### 14 *a. Background*

15 The experiment setup is derived from that used by Aksoy et al. (2009), who simulated  
16 different types of isolated convective storms via assimilation of WSR-88D Z and  $V_r$  observations  
17 on storm-scale domains (i.e., with horizontal dimensions  $\sim 160 - 200$  km) with flat bottom  
18 boundaries. They initialized their model runs with horizontally homogeneous environments  
19 derived from the nearest (in both space and time) available rawinsonde observation (sounding),  
20 populating their initial ensembles by adding perturbations to the wind profiles in these soundings  
21 to account for uncertainty in the rawinsonde measurements.

1           Some discussion about the choice of a horizontally homogeneous model initial  
2 environment (also known as a “single-sounding environment”) is warranted. Stensrud and Gao  
3 (2010), who also performed radar DA experiments on the Greensburg storm, demonstrate the  
4 value of realistic 3D variability in a model initial environment for 1-h forecasts. They conclude  
5 that “knowledge of horizontal environmental variability is important to successful convective-  
6 scale ensemble predictions and needs to be included in real-data experiments.” In light of these  
7 results, Dawson et al. (2012) ruminates on the merits of a horizontally homogeneous model initial  
8 environment, and argue that the single-sounding approach makes sensitivity studies more  
9 straightforward to interpret. Here we focus on assessing the analyses’ sensitivity to assimilation  
10 of different radar data sets and different initial wind profiles, whereas Stensrud and Gao (2010)  
11 focus on prediction of the Greensburg storm.

12           Considering that the Greensburg storm developed on an outflow boundary from a  
13 previous storm (Bluestein 2009), it is accepted that there will be some errors in the analyses  
14 resulting from initial environmental horizontal inhomogeneity that is not accounted for. The  
15 model environment is only horizontally homogeneous at the initial time; forward integration of  
16 the model and DA make the model states horizontally inhomogeneous at all subsequent times.

#### 17           *b. Model initial environment*

18           The initial environment used in this study (Fig. 4), thought to approximate the inflow  
19 environment of the Greensburg storm, was developed in tandem with that used by Dawson et al.  
20 (2012); therefore, many similarities can be seen between their initial environment and ours.

21           The nearest available rawinsonde observation (in both space and time) to the Greensburg  
22 storm was that collected by NWS at 0000 UTC on 5 May 2007 at Dodge City, Kansas (DDC).  
23 This rawinsonde was launched after a dryline passage substantially modified both the wind and

1 thermodynamic profiles below about 800 hPa; they were certainly not representative of the  
2 inflow region of the Greensburg storm. In addition, between 0000 and 0300 UTC, an  
3 intensifying LLJ was observed in velocity-azimuth display (VAD) wind profiles from KDDC  
4 (Fig. 5); this temporal variability was not captured by the single DDC rawinsonde. We chose to  
5 retain the DDC thermodynamic and wind profiles aloft, but made modifications to the near-  
6 surface layers to account for some of the known temporal and spatial variability of the near-  
7 storm environment.

8 From 0000 to 0300 UTC, the nearest well-calibrated, automated surface observation  
9 station (ASOS) to the Greensburg storm is sited at Pratt, Kansas (KPTT), 49 km east of  
10 Greensburg.<sup>2</sup> The forward flank region of the Greensburg storm began to pass over KPTT at  
11 0230 UTC. We assumed that the closest prior KPTT observation (taken at 0210 UTC;  $T = 26$  °C,  
12  $T_d = 19$  °C,  $u = -5$  m s<sup>-1</sup>,  $v = 8$  m s<sup>-1</sup>), was representative of the near-surface inflow environment  
13 of the Greensburg storm. With no more detailed information available about the thermodynamic  
14 characteristics of the boundary layer, we simply inserted a 900 m-deep, well-mixed (constant  $\theta =$   
15 307 K, constant  $q_v = 15$  g kg<sup>-1</sup>) layer. The presence of such a well-mixed boundary layer is  
16 supported by the rawinsonde observation taken at Lamont, Oklahoma at 0000 UTC on 5 May  
17 2007 (not shown), in which a nearly well-mixed layer extended from the surface (317 m MSL) to  
18 1500 m MSL.

19 To test the sensitivity of the analyses to the low-level wind profiles in much the same  
20 manner as Dawson et al. (2012), the velocity-azimuth display (VAD; Browning and Wexler  
21 1968) technique was used to retrieve wind profiles from KDDC  $V_r$  measurements taken at 0100

---

<sup>2</sup> Data from Kansas Groundwater Management District No. 5 evapotranspiration stations, including one located on the north side of Greensburg, were reported as hourly averages (S. Falk, personal communication) and were not suitable for use in these experiments.

1 and 0230 UTC, and these wind profiles were then inserted between the surface and 3000 m  
2 AGL.<sup>3</sup> The Greensburg storm was organizing at 0100 UTC, when the LLJ was weaker, while at  
3 0230 UTC the Greensburg EF-5 tornado was mature, and the LLJ was strengthening. The lowest  
4 useable VAD wind retrieval (at 1090 m MSL, 300 m above KDDC) was linearly interpolated to  
5 the KPTT surface velocity observation.

6 The resulting initial model environment is supportive of supercell thunderstorms, with  
7 4600 J kg<sup>-1</sup> of CAPE (Dawson et al. 2012; their Fig. 1) and 26 m s<sup>-1</sup> (50 kts) of 0 – 6 km bulk  
8 shear (Fig. 5).

### 9 *c. Software*

10 We used NCOMMAS to generate the ensemble of short-term (3 min) forecasts required  
11 by EnKF (Table 3). NCOMMAS is a compressible, non-hydrostatic numerical weather  
12 prediction model designed to simulate atmospheric events in a simplified framework (Coniglio et  
13 al. 2006; Dowell and Wicker 2009). The model employs a 3<sup>rd</sup> order Runge-Kutta advection  
14 scheme with a secondary, shorter time step for acoustic modes (Wicker and Skamarock 2002).  
15 We assimilated radar data using the ensemble square root filter (EnSRF) (Whitaker and Hamill  
16 2002; Dowell et al. 2004b) implementation in NCOMMAS (Dowell and Wicker 2009).

17 Radar observations were assimilated into NCOMMAS as a stream of point observations.  
18 The localization response function (Gaspari and Cohn 1999) for each observation goes to zero at  
19 a horizontal (vertical) radius of 6.0 (3.0) km. The observation operator for  $Z$  is described in the  
20 appendix of Dowell et al. (2011). The observation operator for  $V_r$  is

$$21 \quad v_r = (\sin \alpha \cos \theta_e)u + (\cos \alpha \cos \theta_e)v + (\sin \theta_e)(w - w_t) \quad (1)$$

---

<sup>3</sup> Attempts to retrieve boundary-layer wind profiles from UMass X-Pol data using VAD were unsuccessful because of the narrow ( $\leq 90^\circ$ ) azimuthal sector used.

1 where  $\alpha$  and  $\theta_e$  are the azimuth and elevation angles of the radar beam, respectively,  $(u, v, w)$  is  
2 the model air velocity interpolated to the observation location, and  $w_t$  is the fall speed of  
3 precipitation particles within the grid volume.

4 *d. Radar data editing and objective analysis*

5 In order to reduce the number of radar observations ( $\sim 10^5 - 10^6$  for a single radar sweep)  
6 to a manageable quantity for assimilation, both the KDDC ( $Z$  and  $V_r$ ) and UMass X-Pol ( $V_r$  only)  
7 data from 0030 to 0302 UTC were objectively analyzed to the model horizontal grid spacing  
8 using the Cressman (1959) technique. The radar data were analyzed so that each sweep remained  
9 on its original, conical sweep surface while being horizontally interpolated to the grid (Sun and  
10 Crook 2001; Dowell et al. 2004b), thereby retaining the greater data density in the vertical near  
11 the radars.

12 The KDDC data covered the entire horizontal extent of the model domain. Areas in  
13 which KDDC  $Z$  was greater than or equal to (less than) 20 dBZ were analyzed at 1 km (2 km)  
14 horizontal grid spacing with a radius of influence of 1.5 km (3 km; e.g., Fig. 6a, b). These “low  
15 reflectivity” ( $< 20$  dBZ) observations were analyzed at a coarser horizontal grid spacing so as to  
16 reduce the total number of observations being assimilated, while still retaining enough  
17 information in areas of low  $Z$  (where, presumably, little to no convection is ongoing) to suppress  
18 spurious convection in the model (Caya et al. 2005; Tong and Xue 2005; Aksoy et al. 2009;  
19 Dowell et al. 2011).

20 Assimilation of KDDC data from non-meteorological targets was problematic in  
21 preliminary versions of these experiments. In some cases, the relatively high  $Z$  values associated  
22 with clutter targets (such as wind farms) were erroneously recast by the data-assimilation system  
23 as convective precipitation. To mitigate this issue, KDDC  $Z$  and  $V_r$  data in the lowest three

1 elevation angles ( $0.5^\circ$ ,  $0.9^\circ$ , and  $1.3^\circ$ ) within 30 km of KDDC were omitted from the objective  
2 analysis (e.g., Fig. 6a, b). This practice had the undesirable effect of removing some observations  
3 of real convective precipitation within 30 km of KDDC, at altitudes at or below 680 m AGL.  
4 However, this convective precipitation (which occurred well away from the Greensburg storm)  
5 was not the focus of these experiments, and observations at higher elevation angles helped to  
6 mitigate the effects of these omitted low-altitude data.

7 UMass X-Pol Z data exhibited an attenuation “shadow” from the Greensburg storm’s hail  
8 core resulting from Mie scattering of the X-band signal by large ( $> 4$  cm diameter) hail. (In  
9 accordance with Doviak and Zrnić (1993), we use units of equivalent radar reflectivity,  $\text{dBZ}_e$ , for  
10 the UMass X-Pol Z data.) In addition, these data were not well calibrated for this deployment  
11 (Tanamachi et al. 2012). For these reasons, UMass X-Pol Z data were *not* assimilated;  
12 assimilating them would likely have had the undesired effect of suppressing convection in the  
13 supercell. UMass X-Pol  $V_r$  data associated with uncalibrated Z values less than  $-18 \text{ dBZ}_e$  and that  
14 appeared to contain primarily noise (low Z observations, areas of attenuation) were manually  
15 discarded.<sup>4</sup> These data would be objectively analyzed as near-zero velocity, when in fact there is  
16 simply no reliable information about the velocities in those areas. The resulting UMass X-Pol  $V_r$   
17 field contained only data from the Greensburg storm, and some boundary layer observations near  
18 UMass X-Pol (e.g., Fig. 6c).

#### 19 *e. Model configuration*

20 The experiment setup is summarized in Table 3. The domain, which had 1 km horizontal  
21 grid spacing, was centered slightly southeast of Greensburg, Kansas (Fig. 1) and sufficiently

---

<sup>4</sup> We experimented with several reflectivity and SNR thresholds, but found that manual editing was the most reliable way to retain the desired data near UMass X-Pol while discarding undesired data associated with second trip echo, clutter, and attenuation.

1 large to contain most of the storm between 0100 and 0300 UTC. While a grid with 1 km  
2 horizontal spacing is not generally sufficient to resolve a tornado, the Greensburg tornado was  
3 exceptionally wide, with a maximum damage track width of 2.1 km (Lemon and Umscheid  
4 2008). As will be seen, the minimally-resolved Greensburg tornado, its associated mesocyclone,  
5 and a number of other vortices corresponding to smaller tornadoes are distinct in the resulting  
6 model fields.

7         Within the NCOMMAS simplified experimental framework, no surface fluxes,  
8 turbulence parameterizations, or radiation physics were used. For cloud and precipitation  
9 microphysics, we used the Gilmore et al. (2004) version of the Lin et al. (1983) parameterization  
10 scheme. This single-moment scheme uses five hydrometeor classes, including three ice classes  
11 (cloud ice, snow, and hail/graupel). Large hail was documented in the Greensburg storm  
12 (National Climatic Data Center 2007; Lemon and Umscheid 2008), so relatively high  
13 hail/graupel density ( $\rho_h = 800 \text{ kg m}^{-3}$ ) and low slope intercept parameter ( $N_{0h} = 4 \times 10^4 \text{ m}^{-4}$ ) were  
14 prescribed. It has been found in previous idealized simulations of supercell thunderstorms that a  
15 large intercept parameter for rain (e.g.,  $N_{0r} = 8 \times 10^6 \text{ m}^{-4}$  from Marshall and Palmer (1948),  
16 which has been used in many studies) biases the rain distribution toward small drops and can  
17 result in unrealistically strong cold pools owing to enhanced evaporation (Snook and Xue 2008;  
18 Dawson et al. 2010). Since the presence of large raindrops in the hook and forward flank regions  
19 was inferred from high UMass X-Pol  $Z_{DR}$  measurements (Tanamachi et al. 2012), the intercept  
20 parameter for rain  $N_{0r}$  was prescribed as  $8 \times 10^5 \text{ m}^{-4}$ .

21         To populate the initial (0100 UTC) ensemble of 45 members, and also to account for  
22 instrument and representativeness error in the DDC sounding and KDDC VADs used to generate  
23 the base state environment, random, normally distributed wind components  $\sim N(\bar{v}, \sigma_v) = N(0 \text{ m}$

1  $s^{-1}$ ,  $2.0 \text{ m s}^{-1}$ ) were added to each level of each ensemble member's base state wind profile  
2 (Dowell et al. 2011). The temperature profile (identical in all experiments) was *not* perturbed so  
3 as to avoid inadvertent generation of superadiabatic layers. Small (7.5 km [1.5 km] horizontal  
4 [vertical] radius, 2.0 K) thermal bubbles were then added to each member below 5 km AGL in  
5 regions where the difference between the observed reflectivity and the model reflectivity  
6 exceeded 30 dBZ. Additive noise (described below) was also applied at this time.

7 After advancing the ensemble forward from 0100 UTC to 0112 UTC, objectively  
8 analyzed radar observations were assimilated starting at 0112 UTC. A DA cycle period of 3 min  
9 was chosen as a compromise between the volume update time of KDDC (4.1 min) and that of  
10 UMass X-Pol (~1 min). During assimilation,  $Z$  observations were used to update the  $u$ ,  $v$ ,  $w$ , and  
11 all hydrometeor mixing ratio fields (Dowell et al. 2011);  $V_r$  observations were used to update the  
12 same fields along with the  $\theta$  and water vapor mixing ratio ( $q_v$ ) fields.

13 An additive noise scheme (Caya et al. 2005; Dowell and Wicker 2009) was used to  
14 maintain ensemble spread throughout the assimilation period. Random noise was added to the  
15 model temperature ( $T$ ), dewpoint ( $T_d$ ), and horizontal velocity ( $u$ ,  $v$ ) fields every 6 min in areas  
16 where KDDC  $Z$  was greater than 20 dBZ during the preceding 6 min. The standard deviations of  
17 the noise added to the  $T$ ,  $T_d$ ,  $u$ , and  $v$  field (before smoothing) were prescribed as 1.0 K, 0.5 K,  
18  $2.0 \text{ m s}^{-1}$ , and  $2.0 \text{ m s}^{-1}$ , respectively, and the horizontal (vertical) length scale for smoothing the  
19 perturbations was 4 km (2 km).

20 Three-minute cycling of radar DA, six-minute cycling of additive noise, and six-minute  
21 cycling of small thermal bubble-like perturbations, as described above, were sufficient to  
22 establish the Greensburg storm in the model by 0130 UTC. After 0200 UTC, the thermal bubble-  
23 like perturbations were no longer used.

1 *f. Experiment nomenclature*

2 A total of four EnKF analysis experiments were performed (Table 2), combining two  
3 radar data sets and two wind profiles. In all four experiments, KDDC  $Z$  and  $V_r$  data were  
4 assimilated (Fig. 7), and in two of the four experiments, supplemental UMass X-Pol  $V_r$  data were  
5 also assimilated. These two sets of experiments are distinguished by the descriptive prefixes  
6 “kddc\_only” and “kddc+umass.” It can be seen in Fig. 7(b, c) that many more  $V_r$  observations  
7 were assimilated in the kddc+umass experiments than in the kddc\_only experiments, and that the  
8 number of  $V_r$  observations varied with time, height, and depth of UMass X-Pol volumes (Fig. 2).

9 To represent the effect of the strengthening LLJ on the low-level wind profile, VAD wind  
10 profiles retrieved from KDDC  $V_r$  data were incorporated into the initial velocity profile between  
11 the surface and 3 km AGL. In one set of experiments, the KDDC VAD at 0100 UTC (denoted by  
12 the suffix “vad0100”), prior to the onset of the LLJ, was used, while in the second, the KDDC  
13 VAD from 0230 UTC (suffix “vad0230”), containing a stronger LLJ, was used (Fig. 5).

14 **4. Results**

15 In all four experiments, a robust cyclonic supercell corresponding to the Greensburg  
16 storm was analyzed in the ensemble mean by 0130 UTC, indicating that the assimilation of  
17 KDDC data succeeded in establishing the rotating updraft and precipitation region of the  
18 Greensburg storm (Fig. 8 - Fig. 10). Assimilation of thinned, low  $Z$  observations (Fig. 6a)  
19 suppressed spurious convection in the southern and eastern portions of the domain. An analyzed  
20 near-surface vorticity maximum closely followed the track of the Greensburg tornado in all  
21 ensemble members and can be seen in the ensemble mean (Fig. 10), while the mid-level (2 – 6  
22 km AGL) rotating updraft was evident at 5.3 km AGL (Fig. 11). While many characteristics of

1 the simulated storms were similar, the four experiments exhibited substantial differences,  
2 indicating that both the modification of the near-surface wind profile and the assimilation of the  
3 mobile Doppler radar data impacted the resulting analyses. These differences will be examined  
4 in more detail in the following two subsections.

5 The reader is referred to Dowell and Wicker (2009) for detailed definitions of the  
6 observation-space diagnostic quantities innovation, root mean square of innovations (RMSI),  
7 spread, total spread, and consistency ratio (CR), which we use to quantitatively evaluate the  
8 results. These quantities indicate the change in the model fields as a result of assimilation of  
9 observations and verify that sufficient spread is being maintained in the ensemble. In all four  
10 experiments, the CR of  $V_r$  was less than 1 over most height layers (not shown) from 0112 – 0239  
11 UTC (Fig. 12b), indicating too little model spread relative to the assumed observation errors. It  
12 appears that either our additive noise magnitudes (Section 3e) may have been too small, that our  
13 assumed values for observation error variance (Table 3) were too small, or both. However, we  
14 believe that the individual ensemble members (not shown) exhibit sufficient variability for us to  
15 proceed with the analyses, and that the ensemble means are different enough from one another  
16 for meaningful information to be inferred from them.

#### 17 *a. Assimilation of mobile Doppler radar data*

18 The assimilation of UMass X-Pol observations enabled detailed analysis of supercell  
19 features related to tornado production, including mesocyclones, updrafts, downdrafts, and  
20 surface boundaries such as the rear-flank gust front. All of these features exhibited better  
21 definition in kddc+umass experiments than in kddc\_only experiments.

22 The kddc+umass experiments produced vortices (corresponding to tornadoes) that were  
23 stronger, deeper, and more persistent than those in corresponding kddc\_only experiments (in

1 which UMass X-Pol data were withheld from assimilation) (Fig. 10, Fig. 11). These observations  
2 hold from the genesis through mature phases of the Greensburg tornado (i.e., 0200 - 0250 UTC),  
3 and can be seen in time-height plots of ensemble mean maximum vertical vorticity ( $\zeta$ , Fig. 13)  
4 and vertical velocity ( $w$ , Fig. 14) in the area immediately around the Greensburg storm. Overall,  
5 maximum and average vertical vorticity, and average  $w$ , were larger in kddc+umass experiments  
6 than in corresponding kddc\_only experiments (Fig. 13, Fig. 14). Not only were more  
7 observations assimilated overall in the kddc+umass experiments than in the kddc\_only  
8 experiments, but the assimilated UMass X-Pol  $V_r$  observations were concentrated near the  
9 surface (Fig. 7), where the Greensburg tornado influenced the flow.

10         The most striking differences in the maximum vertical vorticity appear from 0213 – 0233  
11 UTC, when “deep” UMass X-Pol volumes, which contained information throughout the depth of  
12 the mesocyclone(s), were assimilated in the kddc+umass experiments (Fig. 13). Evaluating the  
13 terms in the vertical vorticity tendency equation (e.g., Rotunno and Klemp 1985; Dowell and  
14 Bluestein 2002) near the surface, we found that the stretching term ( $\zeta \frac{\partial w}{\partial z}$ ) was negative near the  
15 Greensburg tornado vortex in kddc\_only experiments, but positive in the kddc+umass  
16 experiments (Fig. 15). Positive near-surface horizontal convergence (and hence, positive vertical  
17 gradient of  $w$ , not shown) in the kddc+umass experiments was responsible for this difference; the  
18 sign of  $\zeta$  in this area was positive in all four experiments. Areas of near-surface horizontal  
19 convergence (divergence) corresponded almost exactly with rising (sinking) motion (Fig. 10), so  
20 the horizontal convergence field is not shown. Some weaker vortices appearing between 0130  
21 and 0145 UTC in the ensemble mean analyses of the kddc+umass\_vad0230 experiment, and  
22 correspond to the incipient/remnant circulations of tornadoes 1-4 (Fig. 16). Tornadoes 1 through  
23 4 were much smaller in scale (< 100 m damage path width) and shorter-lived (~ 4 -13 min) than

1 tornado 5 (Tanamachi et al. 2012). While the core flow in these earlier vortices would have been  
2 unresolvable at 1 km horizontal grid spacing, the vortices influenced the low-level flow fields on  
3 scales resolvable in the analyses. These vortices were less distinct in the kddc+umass\_vad0100  
4 experiment (not shown), and indistinguishable from noise in the kddc\_only experiments (not  
5 shown). Similarly, vortices corresponding to tornadoes 9 and 10 were also analyzed in the  
6 ensemble mean (Fig. 17). However, vorticity maxima associated with tornadoes 6 through 8  
7 (Fig. 2), all short-lived (< 2 min), small (<100 m damage path width) satellites of tornado 5  
8 (Tanamachi et al. 2012), could not be detected in any of the ensemble mean analyses. We  
9 attribute the absence of analyzed vorticity maxima from tornadoes 6-8 to their brevity; none  
10 lasted longer than a single UMass X-Pol volume scan (~90 s).

11 In both the kddc\_only and kddc+umass experiments, the simulated Greensburg storms  
12 developed strong mid-level (2.0 to 6.0 km AGL) updrafts (Fig. 14). Each storm's mid-level  
13 updraft bifurcated into two updrafts between 0215 and 0221 UTC, with the Greensburg tornado's  
14 parent mesocyclone embedded in the western updraft (Fig. 11). The eastern updraft became  
15 stronger than the western updraft by 0239 UTC, causing the eastward propagation of the  
16 Greensburg storm and consequent rearward storm-relative motion of the Greensburg tornado  
17 (Dowell and Bluestein 2002). This change in the Greensburg tornado's storm-relative motion  
18 heralded the onset of its weakening phase, which continued until its demise at 0305 UTC  
19 northwest of Greensburg. The eastern updraft became the parent mesocyclone of a subsequent  
20 EF-3 tornado (T13 in Fig. 2) near Trousdale, Kansas (Lemon and Umscheid 2008). Although the  
21 location and timing of the updraft split are comparable between the experiments, stronger, more  
22 compact mid-level updrafts were analyzed in the kddc+umass experiments than in the kddc\_only

1 experiments (Fig. 11), corresponding with the assimilation of “deep” UMass X-Pol volumes  
2 (Fig. 7).

3         The analyzed low- and mid-level wind fields in the kddc+umass experiments continued  
4 to display major differences from those of the kddc\_only experiments long after the UMass X-  
5 Pol data were no longer available for assimilation (i.e., 0234 – 0300 UTC). In particular, by  
6 0245 UTC, the eastern updraft had developed a much stronger low-level mesocyclone in the  
7 kddc+umass experiments than the kddc\_only experiments (Fig. 18), signifying that the  
8 observations of low- and mid-level mesocyclone cycling contained in the UMass X-Pol data  
9 continued to influence the model forecasts of the mesocyclones’ evolution two or more cycles  
10 (i.e., six or more minutes) after their assimilation. This result concurs with those from Dawson et  
11 al. (2012), who found improvement in free forecasts of the Trousdale mesocyclone initialized at  
12 the start of or during the cycling process versus those initialized before the cycling began.

13         Expanding cold pools were produced in all four experiments, principally beneath the rear  
14 flank downdraft of the Greensburg storm (Fig. 19). We caution against giving too much credence  
15 to the exact temperature values in the cold pools, as no suitable surface data were available for  
16 assimilation or verification. Cold pool strength is often strongly tied to the choice of  
17 microphysical parameterization scheme (e.g., single- versus multi-moment, inclusion versus  
18 exclusion of ice species), and non-linear feedback processes sometimes lead to vastly different  
19 cold pool structures, even when the same scheme is used with slightly different parameter values  
20 (Gilmore et al. 2004; Snook and Xue 2008; Dawson et al. 2010). We used a relatively simple,  
21 single-moment microphysical parameterization scheme (Table 3), but one that does include ice  
22 species. We focus on the *structure* of the cold pool, which we believe is informative.

1           At 0215 UTC, the cold pools (Fig. 19) exhibited a north-northwest-to-south-southeast  
2 oriented boundary separating cooler air in the near-surface portion of the rear-flank downdraft  
3 (RFD) of the Greensburg storm (similar to Fig. 10) from warmer air to its east. In the  
4 kddc+umass experiments, the magnitude of this temperature gradient is larger, and the  
5 accompanying near-surface downdraft stronger, than in the kddc\_only experiments. We conclude  
6 that the assimilation of the UMass X-Pol data makes both analyzed updrafts and downdrafts in  
7 the Greensburg storm stronger and more compact.

8           These changes to the updrafts and downdrafts are accompanied by changes to baroclinic  
9 vorticity generation in the Greensburg storm. Diagnosed baroclinic (solenoidal) generation of  
10 storm-relative streamwise horizontal vorticity (Adlerman et al. 1999) (Fig. 20) is particularly  
11 pronounced along the forward flank gust front (where it is predominantly positive) and along the  
12 rear-flank gust front (where it is predominantly negative, or antistreamwise). We can estimate  
13 the vorticity that might be acquired by a parcel traversing either of these areas. Consider the  
14 kddc+umass\_0230vad experiment (Fig. 20d); a parcel moving westward at  $20 \text{ m s}^{-1}$  through the  
15 forward flank baroclinic zone (which is about 15 km long and has a generation rate of  $0.5 \times 10^{-4}$   
16  $\text{s}^{-2}$ ) could be expected to acquire about  $4 \times 10^{-2} \text{ s}^{-1}$  of streamwise horizontal vorticity, which  
17 could potentially be available for tilting into the vertical once the parcel reached the storm's  
18 updraft (Rotunno and Klemp 1985; Straka et al. 2007). A parcel moving northwestward at  $10 \text{ m}$   
19  $\text{s}^{-1}$  through the baroclinic zone along the along the rear-flank gust front (which is about 7 km  
20 long and has a generation rate of  $1.0 \times 10^{-4} \text{ s}^{-2}$ ) could be expected to acquire about of  $7 \times 10^{-2} \text{ s}^{-1}$   
21 antistreamwise vorticity. We further speculate that if the parcel were subsequently drawn in  
22 towards the tornado, this antistreamwise vorticity could potentially be converted into positive  
23 vertical vorticity by downward tilting of the vortex lines in the RFD (Davies-Jones and Brooks

1 1993; Straka et al. 2007; Marquis et al. 2012). We emphasize that both of these scenarios are  
2 purely speculative; precise calculations of accumulated vorticity along trajectories that would be  
3 needed for confirmation are reserved for a future study incorporating a finer grid.

4 Assimilation of shallow UMass X-Pol volumes (0112 – 0213 UTC) was associated with  
5 increased RMSI (Fig. 12a) and corresponding decreases in the consistency ratio (Fig. 12b) total  
6 spread at and below 6 km relative to the `kddc_only` experiments (Fig. 21). When deep UMass X-  
7 Pol volumes were assimilated (0213 – 0233 UTC), these same effects extended throughout the  
8 model domain depth. We believe these differences in the observation-space diagnostics are  
9 directly attributable to the larger number of observations being assimilated in the `kddc+umass`  
10 experiments, which more strongly constrains the analyses.

11 Zhang et al. (2004), in perfect model experiments simulating a supercell, reported that  
12 assimilating synthetic low-altitude Doppler velocity observations, particularly those from and  
13 below 2 km AGL, improved the retrieved structures and strengths of updrafts, downdrafts, cold  
14 pools, and low-level vorticity maxima relative to experiments in which these data were withheld.  
15 Our results, using real observations, are largely consistent with theirs. Assimilation of more low-  
16 altitude Doppler velocity data (Fig. 7) resulted in more realistic retrievals of supercell features.

#### 17 *b. Modification of initial 0 – 3 km wind profile*

18 The impacts of modifying of the initial 0 – 3 km wind profile are less clear than those  
19 from assimilation of UMass X-Pol data. Differences between the `vad0100` and `vad0230`  
20 experiments include the reflectivity structures of the hook echoes (Fig. 8), the locations and  
21 intensities of vorticity maxima (Fig. 9) and  $w$  maxima (Fig. 10, Fig. 11), and cold pool structure  
22 (Fig. 19).

1           An initial updraft pulse (Fig. 14) at about 0135 UTC and 12 km AGL was stronger (about  
2   85 m s<sup>-1</sup>) in the vad0100 experiments and weaker (about 68 m s<sup>-1</sup>) in the vad0230 experiments.  
3   This initial pulse occurred during the “spin-up” period of the experiment (0100 – 0145 UTC),  
4   when the modeled storm (not shown) bore little resemblance to the real one. Because the real  
5   Greensburg storm (Fig. 1) developed its first intense ( $\geq 60$  dBZ) reflectivity core in less than 4  
6   minutes (between the 0107 and 0111 UTC KDDC volume scans), we consider the rapid  
7   development of the initial updraft pulse realistic.

8           To test the effects of the larger initial low-level shear on a single updraft, we conducted a  
9   simple, single warm bubble test in the vad0100 and vad0230 environments (Fig. 5). The  
10   resulting initial updraft pulse (not shown) was stronger in the vad0100 (weaker shear)  
11   environment than the vad0230 (stronger shear) environment. It appears that the weaker low-level  
12   shear in the vad0100 environment decreased entrainment into the updraft, allowing for a stronger  
13   initial updraft pulse (Weisman and Klemp 1982). Subsequent downdraft pulses (not shown)  
14   originating from the same altitude as the updraft pulse were also stronger in the vad0230  
15   experiments than in the vad0100 experiments, possibly owing to increased entrainment and  
16   evaporation. Given the substantial differences in the simulated storms during the spin-up period,  
17   it is not surprising that the ensemble mean fields are also different at all subsequent times.

18           In the vad0230 experiments, the Greensburg storm produced more “warm” RFD pulses  
19   (in which  $\theta$  was greater than or equal to the base-state temperature, 306.7 K; Fig. 19) than it did  
20   in the vad0100 experiments. Relatively warm RFDs have been associated with significant  
21   tornado production by supercells, possibly because they make more buoyant near-surface air  
22   available to be drawn into tornadoes (Markowski et al. 2002; Grzych et al. 2007). While more  
23   buoyant boundary layer air in the kddc+umass\_vad0230 experiment could help to explain the

1 stronger vorticity maximum when compared to the `kddc+umass_vad0100` experiment, the  
2 vorticity maxima in the corresponding `kddc_only` experiments were comparable in strength with  
3 one another, and the impact of the low-level wind profile was less clear. The assimilation of  
4 UMass X-Pol data in combination with the larger low-level shear in the `vad0230` environment  
5 appears to be the most conducive to the generation of strong vortices.

6 The vorticity maximum corresponding to the Greensburg tornado was stronger, on  
7 average, in the `kddc+umass_vad0230` experiment than in the `kddc+umass_vad0100` experiment  
8 (Fig. 10, Fig. 11, Fig. 13c, d). One would expect the resulting enhancement of the downward-  
9 directed vertical perturbation pressure gradient force inside the stronger vortex to be associated  
10 with weaker updrafts in the `kddc+umass_vad0230` experiment (Fig. 14d) than in the  
11 `kddc+umass_vad0100` experiment (Fig. 14c), and it appears that this is indeed the case.

12 The `vad0230` wind profile had greater low-level vertical wind shear (and hence,  
13 horizontal vorticity) than the `vad0100` wind profile (Fig. 5). In the inflow sector, where the  
14 storm-relative flow was southeasterly, this horizontal vorticity was primarily streamwise at low  
15 levels (Fig. 22), and was continually replenished in the Greensburg storm's inflow sector from  
16 the relatively quiescent southeast quadrant of the model domain. This streamwise vorticity would  
17 have been available for tilting into the vertical by rising motion in the updraft and/or by uplift  
18 along the leading edge of the rear-flank gust front (Fig. 10). All other things being equal, this  
19 process could potentially lead to a stronger analyzed vortex, such as in the `kddc+umass_vad0230`  
20 experiment (Wicker 1996; Shabbott and Markowski 2006). However, a recent study examining  
21 EnKF analyses of multiple tornadoes on finer grids (500 m) indicated that tilting of  
22 baroclinically generated horizontal vorticity may dominate tilting of environmental horizontal  
23 vorticity as a source of vertical vorticity in some tornadoes (Marquis et al. 2012). In our results,

1 baroclinic generation of storm-relative streamwise horizontal vorticity is larger in the  
2 kddc+umass\_vad0230 experiment than in the kddc+umass\_vad0100 experiment (Fig. 20),  
3 lending some credibility to the above scenario. We await future studies in which forward flank  
4 baroclinity in supercells is analyzed through the assimilation of thermodynamic measurements  
5 along with radar data, and more complex microphysical parameterization schemes are employed.

6 As noted in the previous subsection, vorticity maxima associated with some of the  
7 smaller, weaker tornadoes (1-4, 9, and 10) were analyzed in the ensemble mean of the  
8 kddc+umass\_vad0230 experiment (Fig. 16, Fig. 17), but were weaker or absent in the  
9 kddc+umass\_vad0100 experiment (not shown). From these results, we infer that the inclusion of  
10 the LLJ in the initial vad0230 environment did positively impact the development and  
11 maintenance of vortices (relative to the vad0100 environment) throughout the experiment.

## 12 **5. Conclusions**

13 We evaluated the impacts on EnKF analyses of the Greensburg tornadic storm of  
14 assimilation of high-resolution, mobile radar data in an initially horizontally homogeneous  
15 environment. Overall, the additional assimilation of mobile Doppler radar data had a greater  
16 impact on the analyses than did modification of the low-level wind profile, even when these data  
17 were degraded to 1 km horizontal grid spacing and assimilated in 3-minute cycles. (For example,  
18 the kddc+umass\_vad0100 experiment was more similar to the kddc+umass\_vad0230 experiment  
19 than the kddc\_only\_vad0100 experiment.) However, both modifications made differences in the  
20 details of the analyzed storms, in particular the mid-level updraft strength and shape (Fig. 8, Fig.  
21 9, and Fig. 11), cold pool structure (Fig. 19), gust front structure (Fig. 10), vortex strength (Fig.  
22 10, Fig. 13), the presence or absence of vorticity maxima associated with smaller vortices (Fig.

1 17), and baroclinic generation of horizontal vorticity (Fig. 20). All of these features were better  
2 defined in the analyses when UMass X-Pol data were assimilated rather than withheld.

3 Assimilation of UMass X-Pol data primarily impacted areas of the domain where wind  
4 fields had strong spatial gradients and were rapidly evolving (e.g., near gust fronts and intense  
5 vortices; see Fig. 10), resulting in substantial modifications to the inferred kinematics and  
6 dynamics of the Greensburg storm. While this finding is not entirely surprising, it underscores  
7 the relative importance of assimilating observations from multiple, independent platforms,  
8 particularly those collected at low altitudes (Zhang et al. 2004), when attempting to analyze a  
9 highly dynamic atmospheric system such as a tornadic supercell. These results thereby provide  
10 additional justification for efforts to collect radar observations in the 0 – 1 km AGL layer, such  
11 as installing networks of closely spaced, short-range radars (Maki et al. 2008; McLaughlin et al.  
12 2009), and field campaigns like VORTEX2 (Wurman et al. 2012) that incorporate mobile  
13 Doppler radar deployment in severe storms.

14 Analyzed vortices and updrafts were stronger and deeper, especially when “deep” UMass X-  
15 Pol volumes were assimilated. In particular, the stronger horizontal convergence analyzed in the  
16 kddc+umass experiments resulted in a much stronger Greensburg tornado vortex. This outcome  
17 was linked to the sign of the stretching term in the vertical vorticity tendency equation, and, more  
18 tentatively, to enhanced baroclinic generation of horizontal vorticity along gust fronts. The  
19 effects of smaller, more transient vortices associated with tornadoes 1 – 4, 9 and 10 (which  
20 produced damage tracks < 100 m wide) appeared in the ensemble mean of the  
21 kddc+umass\_vad0230 experiment, but inconsistently in other experiments. These tornadoes and  
22 their parent circulations clearly exert influence on scales resolvable in the analyses. The  
23 continued influence of the UMass X-Pol data assimilation was also evident in analyses after

1 UMass X-Pol data were no longer available. In particular, a separate, eastern mesocyclone was  
2 stronger in the kddc+umass experiments than in the kddc\_only experiments at 0245 UTC, more  
3 than 10 minutes after UMass X-Pol data collection ended.

4         There were also significant differences between the vad0230 and vad0100 analyses,  
5 particularly in the kddc+umass experiments. In particular, the analyzed Greensburg tornado  
6 vortex was stronger in the kddc+umass\_vad0230 analyses than in the kddc+umass\_vad0100  
7 analyses, indicating that the analyses were sensitive to the initial model environment for more  
8 than 90 min after assimilation of radar data began. We suggest that while the proper definition of  
9 the model initial environment and the assimilation of near-surface observations are both  
10 important, there may be an “optimal” combination of the two factors that is needed to achieve  
11 high-quality analysis of a supercell in an initially horizontally homogeneous framework. If the  
12 inflow sector is relatively pristine and free from convection (and therefore has lower scatter  
13 concentrations and fewer Doppler velocity observations available for assimilation), as it was in  
14 this case, the conditions there will remain relatively unmodified and continue influence the  
15 development of the supercell throughout the assimilation period. These results are relevant since  
16 horizontally homogeneous initial environments are still used in many modeling studies of severe  
17 storms.

18         Our study focused primarily on the sensitivity of the analyses to different initial conditions  
19 and assimilated data sets. By repeating these experiments on a finer grid (~250 m), saving model  
20 fields more frequently ( $\leq 1$  min), we hope to more fully exploit the high spatial and temporal  
21 resolution of the UMass X-Pol data to diagnose the circulation budget and vortex dynamics of  
22 the Greensburg storm’s mesocyclones and tornadoes using trajectory analyses (e.g., Adlerman et  
23 al. 1999; Markowski et al. 2011a; Marquis et al. 2012). We anticipate that analysis and

1 assimilation of data from novel radar systems, such as polarimetric, phased-array, and / or short-  
2 range, stationary, X-band radars (Jung et al. 2008b; Brewster et al. 2010; Yussouf and Stensrud  
3 2010; Snook et al. 2011; Marquis et al. 2012) will permit fuller exploitation of a greatly  
4 expanded and diversified collection of radar systems in both research and forecasting.

## 5 **Acknowledgments**

6 This research was supported by National Science Foundation grants ATM-0637148, ATM-  
7 0934307, and ATM-0802888, and by NOAA grant NA08OAR4320904. Portions of this  
8 manuscript were completed while the first author was a graduate research assistant at the School  
9 of Meteorology and Cooperative Institute for Mesoscale Meteorological Studies, and  
10 subsequently, a postdoctoral research associate at the Center for Analysis and Prediction of  
11 Storms (CAPS) in Norman, Oklahoma. Sudie Kelly, Glen Romine, and Jeff Anderson at the  
12 National Center for Atmospheric Research (NCAR) in Boulder, Colorado provided visiting  
13 scientist support and assistance with preliminary versions of these experiments.

14 The WSR-88D and NWS automated surface observing station data used in this study were  
15 obtained from the National Climatic Data Center (NCDC). Jeff Hutton of the NWS forecast  
16 office in Dodge City, Kansas provided shape files for the damage tracks that appear in maps.  
17 Kery Hardwick, Vijay Venkatesh, and Dr. Stephen Frasier of MIRSLS processed the UMass X-  
18 Pol data. Conversations with Drs. James Marquis, Chris Snyder, David Stensrud, and George  
19 Bryan were beneficial in the development of the experiments. Feedback from Dr. James Marquis  
20 and another anonymous reviewer strengthened and clarified the manuscript.

21

## References

- 1       **References**
- 2       Adlerman, E. J., K. K. Droegemeier, and R. Davies-Jones, 1999: A numerical simulation of  
3       cyclic mesocyclogenesis. *J. Atmos. Sci.*, **56**, 2045-2069.
- 4       Aksoy, A., D. C. Dowell, and C. Snyder, 2009: A multicaser comparative assessment of the  
5       ensemble Kalman filter for assimilation of radar observations. Part I: Storm-scale analyses.  
6       *Mon. Wea. Rev.*, **137**, 1805-1824.
- 7       Bluestein, H. B., 2009: The formation and early evolution of the Greensburg, Kansas, tornadic  
8       supercell on 4 May 2007. *Wea. Forecasting*, **24**, 899-920.
- 9       Bluestein, H. B., M. M. French, R. L. Tanamachi, S. Frasier, K. Hardwick, F. Junyent, and A. L.  
10       Pazmany, 2007: Close-range observations of tornadoes in supercells made with a dual-  
11       polarization, X-band, mobile Doppler radar. *Mon. Wea. Rev.*, **135**, 1522-1543.
- 12       Brewster, K., K. W. Thomas, J. Gao, J. Brotzge, M. Xue, and Y. Wang, 2010: A nowcasting  
13       system using full physics numerical weather prediction initialized with CASA and NEXRAD  
14       radar data. *25th Conf. on Severe Local Storms*, Denver, Colorado, American Meteorological  
15       Society, 9.4.
- 16       Brown, R. A., V. T. Wood, R. M. Steadham, R. R. Lee, B. A. Flickinger, and D. Sirmans, 2005:  
17       New WSR-88D Volume Coverage Pattern 12: Results of field tests. *Wea. Forecasting*, **20**,  
18       385-393.
- 19       Browning, K. A., and R. Wexler, 1968: The determination of kinematic properties of a wind  
20       field using Doppler radar. *J. Appl. Meteor.*, **7**, 105-113.
- 21       Caya, A., J. Sun, and C. Snyder, 2005: A comparison between the 4DVAR and the ensemble  
22       Kalman filter techniques for radar data assimilation. *Mon. Wea. Rev.*, **133**, 3081-3094.

1 Coniglio, M. C., D. J. Stensrud, and L. J. Wicker, 2006: Effects of upper-level shear on the  
2 structure and maintenance of strong quasi-linear mesoscale convective systems. *J. Atmos.*  
3 *Sci.*, **63**, 1231-1252.

4 Cressman, G. P., 1959: An operational objective analysis system. *Mon. Wea. Rev.*, **87**, 367–374.

5 Davies-Jones, R., and H. E. Brooks, 1993: Mesocyclogenesis from a Theoretical Perspective.  
6 *The Tornado: Its Structure, Dynamics, Prediction, and Hazards, Geophysical Monographs*,  
7 Vol. 79, C. R. Church, D. B. Burgess, C. A. Doswell Iii, and R. Davies-Jones, Eds.,  
8 American Geophysical Union, 105-114.

9 Dawson, D. T., M. Xue, J. A. Milbrandt, and M. K. Yau, 2010: Comparison of evaporation and  
10 cold pool development between single-moment and multimoment bulk microphysics  
11 schemes in idealized simulations of tornadic thunderstorms. *Mon. Wea. Rev.*, **138**, 1152-  
12 1171.

13 Dawson, D. T., L. J. Wicker, E. R. Mansell, and R. L. Tanamachi, 2012: Impact of the  
14 environmental low-level wind profile on ensemble forecasts of the 4 May 2007 Greensburg,  
15 KS tornadic storm and associated mesocyclones. *Mon. Wea. Rev.*, **140**, 696-716.

16 Doviak, R. J., and D. S. Zrnić, 1993: *Doppler Weather Radar and Observations*. 2 ed. Academic  
17 Press, 562 pp.

18 Dowell, D. C., and H. B. Bluestein, 2002: The 8 June 1995 McLean, Texas, storm. Part II:  
19 Cyclic tornado formation, maintenance, and dissipation. *Mon. Wea. Rev.*, **130**, 2649-2670.

20 Dowell, D. C., and L. J. Wicker, 2009: Additive noise for storm-scale ensemble data  
21 assimilation. *J. Atmos. Oceanic Technol.*, **26**, 911-927.

22 Dowell, D. C., L. J. Wicker, and D. J. Stensrud, 2004a: High resolution analyses of the 8 May  
23 2003 Oklahoma City storm. Part II: EnKF data assimilation and forecast experiments. *22nd*

1       *Conf. on Severe Local Storms*, Hyannis, Massachusetts, American Meteorological Society,  
2       12.15.

3       Dowell, D. C., L. J. Wicker, and C. Snyder, 2011: Ensemble Kalman filter assimilation of radar  
4       observations of the 8 May 2003 Oklahoma City supercell: Influences of reflectivity  
5       observations on storm-scale analyses. *Mon. Wea. Rev.*, **139**, 272–294.

6       Dowell, D. C., F. Zhang, L. J. Wicker, C. Snyder, and N. A. Crook, 2004b: Wind and  
7       temperature retrievals in the 17 May 1981 Arcadia, Oklahoma, supercell: Ensemble Kalman  
8       filter experiments. *Mon. Wea. Rev.*, **132**, 1982–2005.

9       Evensen, G., 1994: Sequential data assimilation with a nonlinear quasi-geostrophic model using  
10       Monte Carlo methods to forecast error statistics. *J. Geophys. Res.*, **99**, 10143–10162.

11       French, M. M., 2006: The 15 May 2003 Shamrock, Texas, supercell : A dual-Doppler analysis  
12       and EnKF data assimilation experiment. M.S. Thesis, School of Meteorology, University of  
13       Oklahoma, 145 pp.

14       French, M. M., H. B. Bluestein, D. C. Dowell, L. J. Wicker, M. R. Kramar, and A. L. Pazmany,  
15       2006: The 15 May 2003 Shamrock, Texas, supercell: A dual-Doppler analysis and EnKF  
16       data-assimilation experiment. *23rd Conf. on Severe Local Storms*, St. Louis, Missouri,  
17       American Meteorological Society, 14.16A.

18       Gaspari, G., and S. E. Cohn, 1999: Construction of correlation functions in two and three  
19       dimensions. *Quart. J. Roy. Meteor. Soc.*, **125**, 723–757.

20       Gilmore, M. S., J. M. Straka, and E. N. Rasmussen, 2004: Precipitation and evolution sensitivity  
21       in simulated deep convective storms: Comparisons between liquid-only and simple ice and  
22       liquid phase microphysics. *Mon. Wea. Rev.*, **132**, 1897–1916.

1 Grzych, M. L., B. D. Lee, and C. A. Finley, 2007: Thermodynamic analysis of supercell rear-  
2 flank downdrafts from Project ANSWERS. *Mon. Wea. Rev.*, **135**, 240-246.

3 Houtekamer, P. L., and H. L. Mitchell, 1998: Data assimilation using an ensemble Kalman filter  
4 technique. *Mon. Wea. Rev.*, **126**, 796-811.

5 Jung, Y., G. Zhang, and M. Xue, 2008a: Assimilation of simulated polarimetric radar data for a  
6 convective storm using the ensemble Kalman filter. Part I: Observation operators for  
7 reflectivity and polarimetric variables. *Mon. Wea. Rev.*, **136**, 2228-2245.

8 Jung, Y., M. Xue, G. Zhang, and J. M. Straka, 2008b: Assimilation of simulated polarimetric  
9 radar data for a convective storm using the ensemble Kalman filter. Part II: Impact of  
10 polarimetric data on storm analysis. *Mon. Wea. Rev.*, **136**, 2246-2260.

11 Kain, J. S., M. Xue, M. C. Coniglio, S. J. Weiss, F. Kong, T. L. Jensen, B. G. Brown, J. Gao, K.  
12 Brewster, K. W. Thomas, Y. Wang, C. S. Schwartz, and J. J. Levit, 2010: Assessing  
13 advances in the assimilation of radar data and other mesoscale observations within a  
14 collaborative forecasting–research environment. *Wea. Forecasting*, **25**, 1510-1521.

15 Lemon, L. R., and M. Umscheid, 2008: The Greensburg, KS tornadic storm: a storm of  
16 extremes. *24th Conf. on Severe Local Storms*, Savannah, Georgia, American Meteorological  
17 Society, 2.4.

18 Lilly, D. K., 1990: Numerical prediction of thunderstorms—has its time come? *Quart. J. Roy.*  
19 *Meteor. Soc.*, **116**, 779-798.

20 Lin, Y.-L., R. D. Farley, and H. D. Orville, 1983: Bulk parameterization of the snow field in a  
21 cloud model. *J. Appl. Meteor.*, **22**, 1065-1092.

22 Maki, M., T. Maesaka, R. Misumi, K. Iwanami, S.-i. Suzuki, A. Kato, S. Shimizu, K. Kieda, T.  
23 Yamada, H. Hirano, F. Kobayashi, A. Masuda, T. Moriya, Y. Suzuki, A. Takahori, D.-I. Lee,

1 D.-S. Kim, V. Chandrasekar, and Y. Wang, 2008: X-band Polarimetric Radar Network in the  
2 Tokyo Metropolitan Area - X-NET. *5th European Conf. on Radar Meteorology and*  
3 *Hydrology*, Finland, Finnish Meteorological Institute, 5.

4 Markowski, P., Y. Richardson, J. Wurman, K. Kosiba, P. Robinson, and J. Marquis, 2011a:  
5 Observations from VORTEX2: The pretornadic phase of the Goshen County, Wyoming,  
6 supercell (5 June 2009). *35th Conf. on Radar Meteorology*, Pittsburgh, Pennsylvania,  
7 American Meteorological Society, 8B.1.

8 Markowski, P. M., J. M. Straka, and E. N. Rasmussen, 2002: Direct surface thermodynamic  
9 observations within the rear-flank downdrafts of nontornadic and tornadic supercells. *Mon.*  
10 *Wea. Rev.*, **130**, 1692-1721.

11 Markowski, P. M., M. Majcen, Y. Richardson, J. Marquis, and J. Wurman, 2011b:  
12 Characteristics of the wind field in a trio of nontornadic low-level mesocyclones observed by  
13 the Doppler On Wheels radars. *Electronic J. Severe Storms Meteor.*, **6**, 1-48.

14 Marquis, J., Y. Richardson, J. Wurman, and P. Markowski, 2008: Single- and dual-Doppler  
15 analysis of a tornadic vortex and surrounding storm-scale flow in the Crowell, Texas,  
16 supercell of 30 April 2000. *Mon. Wea. Rev.*, **136**, 5017-5043.

17 Marquis, J., Y. Richardson, P. Markowski, D. Dowell, and J. Wurman, 2012: Tornado  
18 maintenance investigated with high-resolution dual-Doppler and EnKF analysis. *Mon. Wea.*  
19 *Rev.*, **140**, 3-27.

20 Marquis, J., Y. Richardson, P. M. Markowski, D. C. Dowell, J. Wurman, K. Kosiba, and P.  
21 Robinson, 2010: Preliminary analysis of the Goshen County tornadic supercell on 5 June  
22 2009 during VORTEX2 using EnKF assimilation of mobile radar and mesonet data. *25th*  
23 *Conf. on Severe Local Storms*, Denver, Colorado, American Meteorological Society, 6.7.

1 Marshall, J. S., and W. M. K. Palmer, 1948: The distribution of raindrops with size. *J. Meteor.*,  
2 **5**, 165-166.

3 McLaughlin, D., D. Pepyne, B. Philips, J. Kurose, M. Zink, D. Westbrook, E. Lyons, E. Knapp,  
4 A. Hopf, A. Defonzo, R. Contreras, T. Djaferis, E. Insanic, S. Frasier, V. Chandrasekar, F.  
5 Junyent, N. Bharadwaj, Y. Wang, Y. Liu, B. Dolan, K. Droegemeier, J. Brotzge, M. Xue, K.  
6 Kloesel, K. Brewster, F. Carr, S. Cruz-Pol, K. Hondl, and P. Kollias, 2009: Short-wavelength  
7 technology and the potential for distributed networks of small radar systems. *Bull. Amer.*  
8 *Meteor. Soc.*, **90**, 1797-1817.

9 Monfredo, W., 2008: Blown away in Greensburg, USA: prediction and analysis of an EF-5  
10 tornado. *Weather*, **63**, 116-120.

11 National Climatic Data Center, 2007: Storm Events Database. [http://www4.ncdc.noaa.gov/cgi-](http://www4.ncdc.noaa.gov/cgi-win/wwcgi.dll?wwEvent~Storms)  
12 [win/wwcgi.dll?wwEvent~Storms](http://www4.ncdc.noaa.gov/cgi-win/wwcgi.dll?wwEvent~Storms), retrieved on 12 January 2009.

13 National Research Council, 1995: *Assessment of Nexrad Coverage and Associated Weather*  
14 *Services*. Washington, D.C., 104 pp.

15 Oye, R., C. Mueller, and S. Smith, 1995: Software for radar translation, visualization, editing,  
16 and interpolation. *27th Conf. on Radar Meteorology*, Vail, Colorado, American  
17 Meteorological Society, 359 - 361.

18 Rotunno, R., and J. Klemp, 1985: On the rotation and propagation of simulated supercell  
19 thunderstorms. *J. Atmos. Sci.*, **42**, 271-292.

20 Shabbott, C. J., and P. M. Markowski, 2006: Surface in situ observations within the outflow of  
21 forward-flank downdrafts of supercell thunderstorms. *Mon. Wea. Rev.*, **134**, 1422-1441.

22 Snook, N. A., and M. Xue, 2008: Effects of microphysical drop size distribution on  
23 tornadogenesis in supercell thunderstorms. *Geophys. Res. Lett.*, **35**, L28403.

1 Snook, N. A., M. Xue, and Y. Jung, 2011: Analysis of a tornadic mesoscale convective vortex  
2 assimilating CASA X-band and WSR-88D radar data using an ensemble Kalman filter. *Mon.*  
3 *Wea. Rev.*, **139**, 3446-3468.

4 Snyder, C., and F. Zhang, 2003: Assimilation of simulated Doppler radar observations with an  
5 ensemble Kalman filter. *Mon. Wea. Rev.*, **131**, 1663-1677.

6 Stensrud, D. J., and J. Gao, 2010: Importance of horizontally inhomogeneous environmental  
7 initial conditions to ensemble storm-scale radar data assimilation and very short-range  
8 forecasts. *Mon. Wea. Rev.*, **138**, 1250-1272.

9 Stensrud, D. J., L. J. Wicker, K. E. Kelleher, M. Xue, M. P. Foster, J. T. Schaefer, R. S.  
10 Schneider, S. G. Benjamin, S. S. Weygandt, J. T. Ferree, and J. P. Tuell, 2009: Convective-  
11 scale Warn-on-Forecast system. *Bull. Amer. Meteor. Soc.*, **90**, 1487-1499.

12 Straka, J. M., E. N. Rasmussen, R. P. Davies-Jones, and P. M. Markowski, 2007: An  
13 observational and idealized numerical examination of low-level counter-rotating vortices in  
14 the rear flank of supercells. *Electronic J. Severe Storms Meteor.*, **2**, 1-22.

15 Sun, J., 2005: Convective-scale assimilation of radar data: progress and challenges. *Quart. J.*  
16 *Roy. Meteor. Soc.*, **131**, 3439-3463.

17 Sun, J., and N. A. Crook, 2001: Real-time low-level wind and temperature analysis using single  
18 WSR-88D data. *Wea. Forecasting*, **16**, 117-132.

19 Tanamachi, R. L., H. B. Bluestein, J. B. Houser, K. M. Hardwick, and S. J. Frasier, 2012:  
20 Mobile, X-band, polarimetric Doppler radar observations of the 4 May 2007 Greensburg,  
21 Kansas tornadic supercell. *Mon. Wea. Rev.*, **140**, 2103-2125.

22 Tong, M., and M. Xue, 2005: Ensemble Kalman filter assimilation of Doppler radar data with a  
23 compressible nonhydrostatic model: OSS experiments. *Mon. Wea. Rev.*, **133**, 1789-1807.

1 Weisman, M. L., and J. B. Klemp, 1982: The dependence of numerically simulated convective  
2 storms on vertical wind shear and buoyancy. *Mon. Wea. Rev.*, **110**, 504-520.

3 Whitaker, J. S., and T. M. Hamill, 2002: Ensemble data assimilation without perturbed  
4 observations. *Mon. Wea. Rev.*, **130**, 1913-1924.

5 Wicker, L. J., 1996: The role of near surface wind shear on the generation of low-level  
6 mesocyclones and tornadoes. *18th Conf. on Severe Local Storms*, San Francisco, California,  
7 American Meteorological Society, 115-119.

8 Wicker, L. J., and W. C. Skamarock, 2002: Time-splitting methods for elastic models using  
9 forward time schemes. *Mon. Wea. Rev.*, **130**, 2088-2097.

10 Wurman, J., K. Kosiba, P. Markowski, Y. Richardson, D. Dowell, and P. Robinson, 2010:  
11 Finescale single- and dual-Doppler analysis of tornado intensification, maintenance, and  
12 dissipation in the Orleans, Nebraska, supercell. *Mon. Wea. Rev.*, **138**, 4439-4455.

13 Wurman, J., D. Dowell, Y. Richardson, P. Markowski, E. Rasmussen, D. Burgess, L. Wicker,  
14 and H. B. Bluestein, 2012: The Second Verification of the Origins of Rotation in Tornadoes  
15 Experiment: VORTEX2. *Bull. Amer. Meteor. Soc.*, in press.

16 Yussouf, N., and D. J. Stensrud, 2010: Impact of phased-array radar observations over a short  
17 assimilation period: Observing system simulation experiments using an ensemble Kalman  
18 filter. *Mon. Wea. Rev.*, **138**, 517-538.

19 Zhang, F., C. Snyder, and J. Sun, 2004: Impacts of initial estimate and observation availability  
20 on convective-scale data assimilation with an ensemble Kalman filter. *Mon. Wea. Rev.*, **132**,  
21 1238-1253.

22  
23

1       **List of figures**

2       Fig. 1. (a) Model domain (outlined in blue) and objectively analyzed KDDC reflectivity (in dBZ)  
3       at 1.0 km AGL within that domain at (b) 0100 UTC, (c) 0130 UTC, (d) 0200 UTC, (e) 0230  
4       UTC, and (f) 0300 UTC on 5 May 2007. Distances (in km) are relative to the southwest  
5       corner of the model domain. Thin gray (heavy black) lines denote county (state) boundaries.  
6       Surveyed tornado damage tracks (outlined in purple) are courtesy of J. Hutton of the NWS  
7       forecast office in Dodge City, Kansas.

8       Fig. 2. Timeline of Greensburg storm, tornadoes and radar data collection. Start times of KDDC  
9       volumes are shown as tick marks. Tornadoes are numbered chronologically (following  
10      Lemon and Umscheid 2008). For UMass X-Pol deployment times, dashed lines indicate  
11      times when single-elevation scans were collected; the solid line indicates when “shallow”  
12      volume scans were collected, and the thick bar indicates when “deep” volume scans were  
13      collected.

14      Fig. 3. Side-by-side comparisons of (a, b)  $Z$  and (c, d)  $V_r$  data collected at 0230 UTC (when  
15      tornado 5 was mature) by (a, c) KDDC at  $0.5^\circ$  and (b, d) UMass X-Pol at  $2.9^\circ$ . All panels use  
16      the same scale and are centered on the vortex. Range rings are every 15 km. UMass X-Pol  
17      reflectivity was attenuated on the north side of the Greensburg storm because of large hail in  
18      the storm core;  $V_r$  data in this region were manually excluded.  $V_r$  data were manually  
19      dealiasied. UMass X-Pol  $V_r$  data were further edited to exclude “noisy” velocity data outside  
20      the storm, but some gates close to the radar, which contain information about the near-  
21      surface wind fields, were retained.

22      Fig. 4. Observations used in the construction of the model initial environment. Heights and  
23      distances between observing platforms are not to scale.

1 Fig. 5. Hodographs of the initial wind profiles used in the EnKF experiments prior to  
2 interpolation to the model grid levels. The black (gray) curve depicts the “vad0230”  
3 (“vad0100”) wind profile. Greensburg storm motion is denoted by a dark gray cross. Altitude  
4 labels are in km AGL. The surface velocity components are from the KPTT observation at  
5 0210 UTC on 5 May 2007, while those in the 0.3 – 3.0 km layer are from KDDC VAD  
6 retrievals. The wind profiles above 3.0 km are from the 5 May 2007, 0000 UTC DDC  
7 sounding and are identical for both experiments.

8 Fig. 6. Objectively analyzed KDDC (a) reflectivity (in dBZ) and (b) Doppler velocity (in  $\text{m s}^{-1}$ )  
9 collected at 0229 UTC at an elevation angle of  $0.5^\circ$ , and (c) objectively analyzed UMass X-  
10 Pol Doppler velocity (in  $\text{m s}^{-1}$ ) collected at 0230 UTC at an elevation angle of  $2.9^\circ$ . KDDC  
11 observations associated with reflectivity values greater than or equal to (less than) 20 dBZ  
12 were analyzed at 1 km (2 km) grid spacing. The dashed purple circle denotes the 30 km range  
13 ring around KDDC; data inside this radius were discarded for the lowest three elevation  
14 angles ( $0.5^\circ$ ,  $0.9^\circ$ , and  $1.3^\circ$ ) in each volume in order to avoid ground clutter targets.

15 Fig. 7. Number of (a)  $Z$  and (b, c)  $V_r$  observations (e.g., Fig. 6) available for assimilation as a  
16 function of time and altitude. UMass X-Pol  $Z$  observations are not shown because they were  
17 not assimilated; the  $Z$  observations are only from KDDC and are the same for all  
18 experiments. Times when UMass X-Pol collected shallow and deep volumes (Fig. 2) are  
19 delineated in panel (c). Observations are plotted in 4-minute bins for clarity. The movement  
20 out of the domain of the Greensburg storm (as well as other storms) explains the overall  
21 decrease with time of both KDDC  $Z$  and  $V_r$  observations.

22 Fig. 8. Prior ensemble mean reflectivity (in dBZ) at 0.8 km AGL at 0200 UTC (when the  
23 Greensburg tornado formed) for experiments (a) `kddc_only_vad0100`, (b)

1 kddc\_only\_vad0230, (c) kddc+umass\_vad0100, and (d) kddc+umass\_vad0230. County  
2 boundaries are drawn in gray; tornado damage tracks are outlined in purple.

3 Fig. 9. As in Fig. 8, but at 0230 UTC (when the Greensburg tornado was mature).

4 Fig. 10. As in Fig. 9, but slightly enlarged and showing prior ensemble mean vertical velocity  
5 (colored shading in  $\text{m s}^{-1}$ ), vorticity (solid black contours in  $10^{-3} \text{ s}^{-1}$ , starting from  $10 \times 10^{-3} \text{ s}^{-1}$   
6  $^1$ ), reflectivity (gray contours at 35 and 55 dBZ), and storm-relative velocity vectors (drawn  
7 every 2 km).

8 Fig. 11. As in Fig. 10, but at 5.3 km AGL.

9 Fig. 12.  $V_r$  (a) RMSI (solid), mean innovation (dotted), and ensemble spread (dashed; in  $\text{m s}^{-1}$ )  
10 and (b) consistency ratio (unitless). In panel (a), a horizontal dashed line marks  $\sigma_{V_r} = 3.0 \text{ m s}^{-1}$   
11  $^1$ . In panel (b), a horizontal dashed line marks unity. Vertical purple lines mark the start and  
12 end of UMass X-Pol volumetric data collection (Fig. 7); the dashed line marks when UMass  
13 X-Pol switched from collecting “shallow” to “deep” volumes.

14 Fig. 13. Time-height plot of prior ensemble mean maximum vertical vorticity (in  $10^{-3} \text{ s}^{-1}$ ) for  
15 experiments (a) kddc\_only\_vad0100, (b) kddc\_only\_vad0230, (c) kddc+umass\_vad0100, and  
16 (d) kddc+umass\_vad0230. Vertical purple lines mark changes in UMass X-Pol volumetric  
17 data collection as in Fig. 12.

18 Fig. 14. As in Fig. 13, but for ensemble mean maximum vertical velocity (in  $\text{m s}^{-1}$ ).

19 Fig. 15. As in Fig. 9, but showing the stretching term of the vertical vorticity tendency equation  
20 (in  $10^{-4} \text{ s}^{-2}$ ). Note that the panels are enlarged relative to those in Fig. 9, and that velocity  
21 vectors are drawn every 1 km.

22 Fig. 16. (a) Ensemble mean analyzed vertical vorticity (colored shading), with solid black  
23 contours plotted at  $8 \times 10^{-3} \text{ s}^{-1}$  and  $10 \times 10^{-3} \text{ s}^{-1}$ , reflectivity (gray contours at 35 and 55 dBZ),

1 and storm-relative velocity vectors (plotted at 2 km intervals) at 1.3 km AGL for the  
2 kddc+umass\_vad0230 experiment. Only positive values of vertical vorticity are plotted in  
3 panel (a), and the outline of the UMass X-Pol sector is overlaid. (b) UMass X-Pol  
4 uncalibrated reflectivity (in dBZ) and (c) Doppler velocity (in  $\text{m s}^{-1}$ ) at an elevation angle of  
5  $4.3^\circ$ . Vertical vorticity maxima and circulations corresponding to tornadoes are circled and  
6 numbered as in Lemon and Umscheid (2008). At this time (0145 UTC), tornado 1 was  
7 dissipating, tornado 2 had already dissipated into a remnant vortex, tornado 3 was  
8 developing, and tornado 4's vortex was forming above the  $4.3^\circ$  elevation angle sweep  
9 surface.

10 Fig. 17. (a) Ensemble mean analyzed vertical vorticity (colored shading) with solid black  
11 contours plotted at  $-10 \times 10^{-3} \text{ s}^{-1}$  (dashed) and at intervals of  $10 \times 10^{-3} \text{ s}^{-1}$  starting at  $10 \times 10^{-3} \text{ s}^{-1}$   
12  $^1$  (solid), reflectivity (gray contours at 35 and 55 dBZ), and storm-relative velocity vectors  
13 (plotted at 2 km intervals) at 2.3 km AGL at 0224 UTC for the kddc+umass\_vad0230  
14 experiment. (b) UMass X-Pol uncalibrated reflectivity (in dBZ) and (c) Doppler velocity (in  
15  $\text{m s}^{-1}$ ) at an elevation angle of  $10.4^\circ$  at 0221 UTC. Vertical vorticity maxima and circulations  
16 corresponding to tornadoes are circled and numbered as in Lemon and Umscheid (2008).  
17 Note that tornado 9 was anticyclonic.

18 Fig. 18. As in Fig. 10, but at 0245 UTC, 2.3 km AGL, and shifted slightly northeast.

19 Fig. 19. Ensemble mean perturbation potential temperature (color shading, in K) at 0.3 km AGL  
20 (the model level closest to the surface), vertical vorticity (solid black contours) at intervals of  
21  $10 \times 10^{-3} \text{ s}^{-1}$  starting at  $10 \times 10^{-3} \text{ s}^{-1}$ , reflectivity (gray contours at 35 and 55 dBZ), and storm-  
22 relative velocity vectors (plotted at 2 km intervals) at 0215 UTC. Potential temperatures are  
23 plotted relative to the initial model state ( $\theta=306.7 \text{ K}$ ).

1 Fig. 20. As in Fig. 15, but showing the ensemble mean baroclinic generation of storm-relative  
2 streamwise horizontal vorticity (in  $10^{-4} \text{ s}^{-2}$ ) at 0215 UTC. Note that the panels are  
3 compressed and shifted relative to those in Fig. 15.

4 Fig. 21. Layer-averaged total spread (in  $\text{m s}^{-1}$ ) over the entire domain for experiments (a)  
5 kddc\_only\_vad0100, (b) kddc\_only\_vad0230, (c) kddc+umass\_vad0100, and (d)  
6 kddc+umass\_vad0230. Vertical purple lines mark changes in UMass X-Pol volumetric data  
7 collection as in Fig. 12. White rectangles denote regions where statistically insignificant  
8 number of observations were assimilated.

9 Fig. 22. Vertical profiles of storm-relative streamwise horizontal vorticity associated with the  
10 hodographs depicted in Fig. 5.

11

12

1      **Tables**

2              Table 1. Characteristics of KDDC and UMass X-Pol radars in 2007.

<b>Radar</b>	<b>KDDC (WSR-88D)</b>	<b>UMass X-Pol</b>
Type	Stationary	Mobile
Wavelength	10 cm	3 cm
Half-power beamwidth	1.0°	1.2°
Peak transmitted power	475 kW	25 kW
Max. unambiguous range	231 km	75 km
Max. unambiguous velocity	32.5 m s <sup>-1</sup>	19.2 m s <sup>-1</sup>
Range gate spacing	1 km (Z), 250 m (v <sub>r</sub> )	150 m
Max. azimuthal scan rate	30° s <sup>-1</sup>	24° s <sup>-1</sup>
Polarimetry	Single	Dual

3

4

1

Table 2. Experiment naming convention.

<b>Experiment name</b>	<b>“Weaker LLJ”</b>	<b>“Stronger LLJ”</b>
<b>KDDC <math>Z</math> and <math>V_r</math> data assimilated</b>	kddc_only_vad0100	kddc_only_vad0230
<b>KDDC <math>Z</math> and <math>V_r</math> and UMass <math>V_r</math> data assimilated</b>	kddc+umass_vad0100	kddc+umass_vad0230

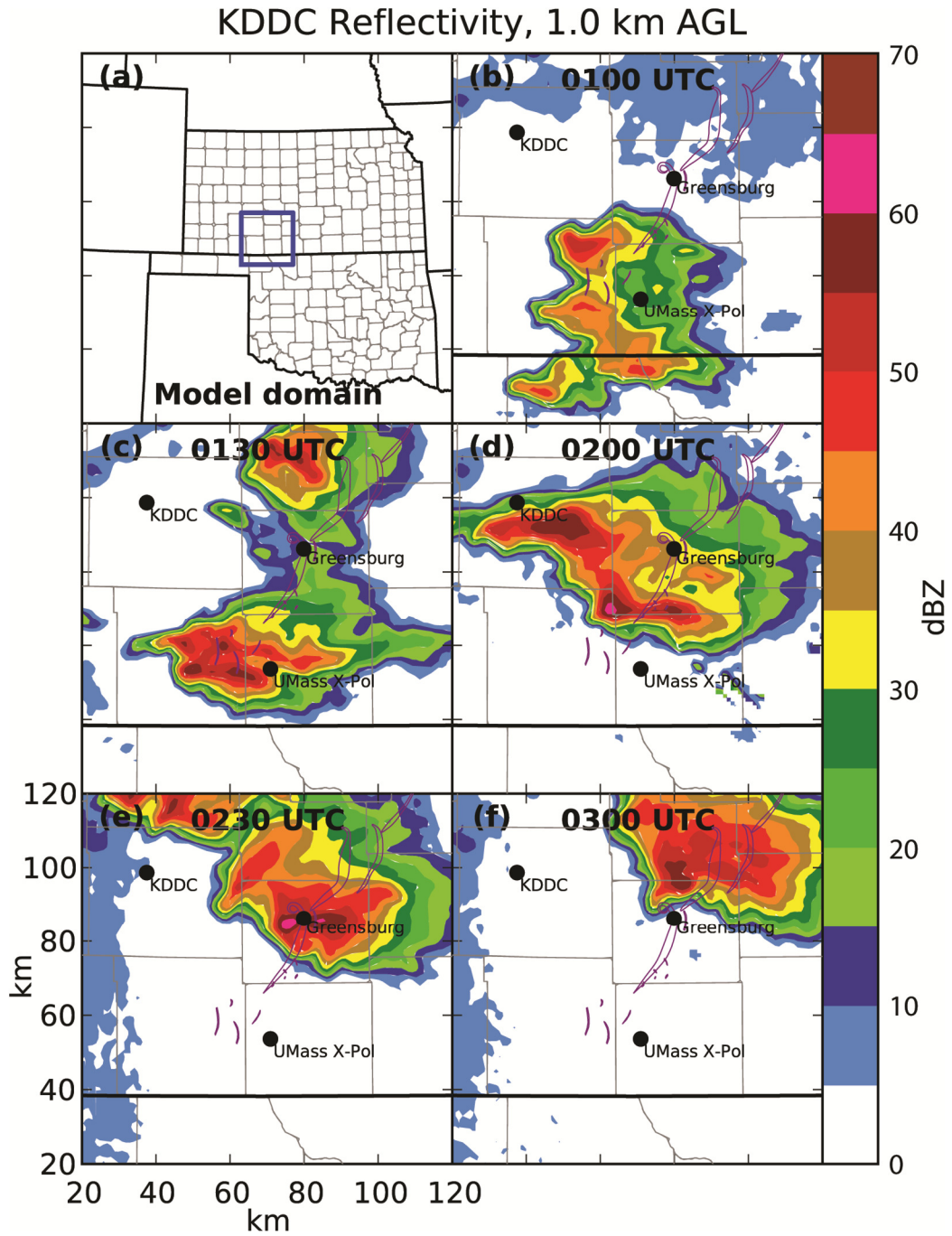
2

3

Table 3. List of model parameters.

<b>Parameter</b>	<b>Value</b>
Model initial time	0030 UTC, 5 May 2007
Assimilation window	0100 – 0300 UTC, 5 May 2007
Assimilation cycle frequency	3 min
Ensemble members	45
Simulation domain	140 km × 140 km × 20 km
Domain size	141 × 141 × 41
Center of domain	37.58 °N, 99.22 °W
Model bottom boundary	650 m MSL
Horizontal grid spacing	1 km
Vertical grid spacing	500 m (First scalar level 250 m AGL)
Cloud microphysical scheme	Lin-Farley-Orville (Gilmore et al. 2004)
Rain density ( $\rho_r$ )	1000 kg m <sup>-3</sup>
Rain intercept parameter ( $N_{0r}$ )	$8.0 \times 10^5$ m <sup>-4</sup>
Hail/graupel density ( $\rho_h$ )	800 kg m <sup>-3</sup>
Hail/graupel intercept parameter ( $N_{0h}$ )	$4.0 \times 10^4$ m <sup>-4</sup>
Snow density ( $\rho_s$ )	100 kg m <sup>-3</sup>
Snow intercept parameter ( $N_{0s}$ )	$3.0 \times 10^6$ m <sup>-4</sup>
Lateral boundaries	Open
Model time step	3 sec
Assumed observation error variance for $Z$ ( $\sigma_z^2$ ) and $V_r$ ( $\sigma_{vr}^2$ )	(5.0 dBZ) <sup>2</sup> , (3.0 m s <sup>-1</sup> ) <sup>2</sup>

1 **Figures**



2

3

4

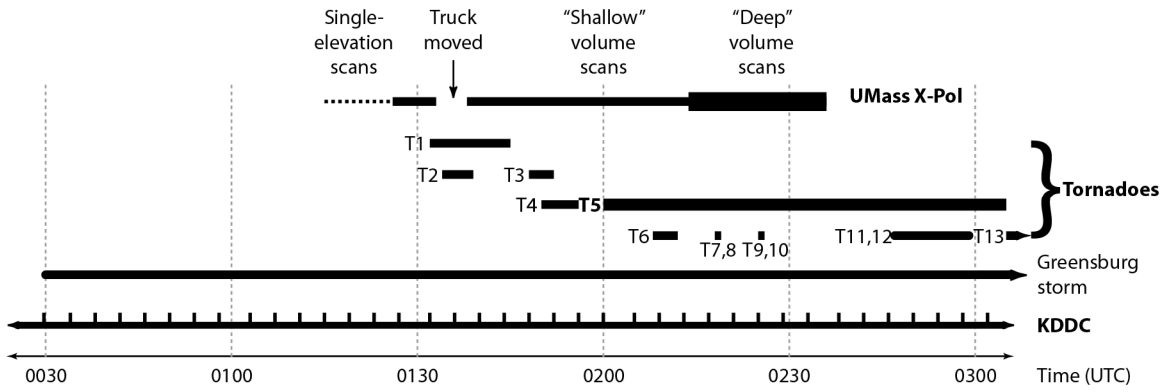
5

6

7

8

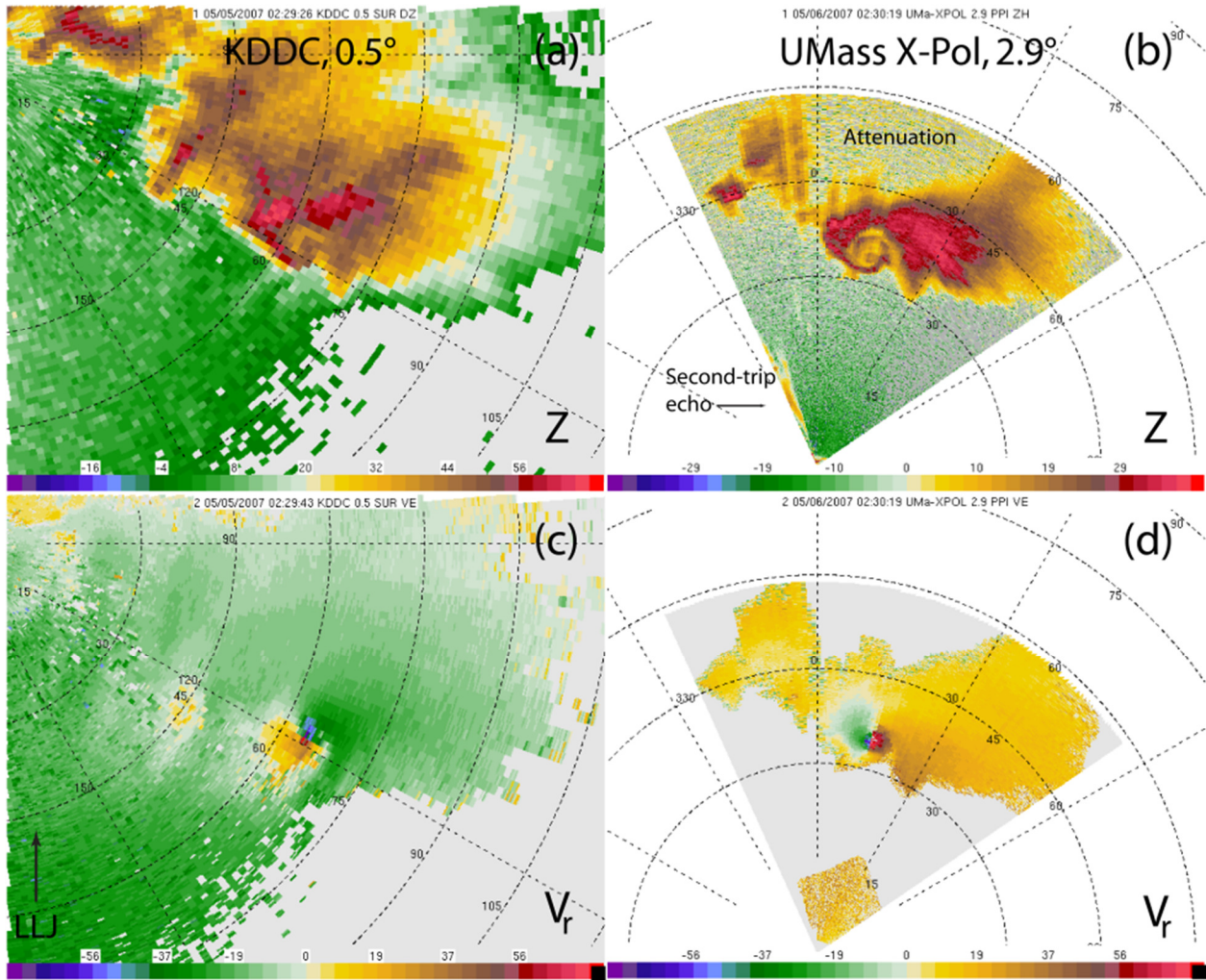
Fig. 1. (a) Model domain (outlined in blue) and objectively analyzed KDDC reflectivity (in dBZ) at 1.0 km AGL within that domain at (b) 0100 UTC, (c) 0130 UTC, (d) 0200 UTC, (e) 0230 UTC, and (f) 0300 UTC on 5 May 2007. Distances (in km) are relative to the southwest corner of the model domain. Thin gray (heavy black) lines denote county (state) boundaries. Surveyed tornado damage tracks (outlined in purple) are courtesy of J. Hutton of the NWS forecast office in Dodge City, Kansas.



1  
2  
3  
4  
5  
6  
7

Fig. 2. Timeline of Greensburg storm, tornadoes and radar data collection. Start times of KDDC volumes are shown as tick marks. Tornadoes are numbered chronologically (following Lemon and Umscheid 2008). For UMass X-Pol deployment times, dashed lines indicate times when single-elevation scans were collected; the solid line indicates when "shallow" volume scans were collected, and the thick bar indicates when "deep" volume scans were collected.

1



2

3

4

5

6

7

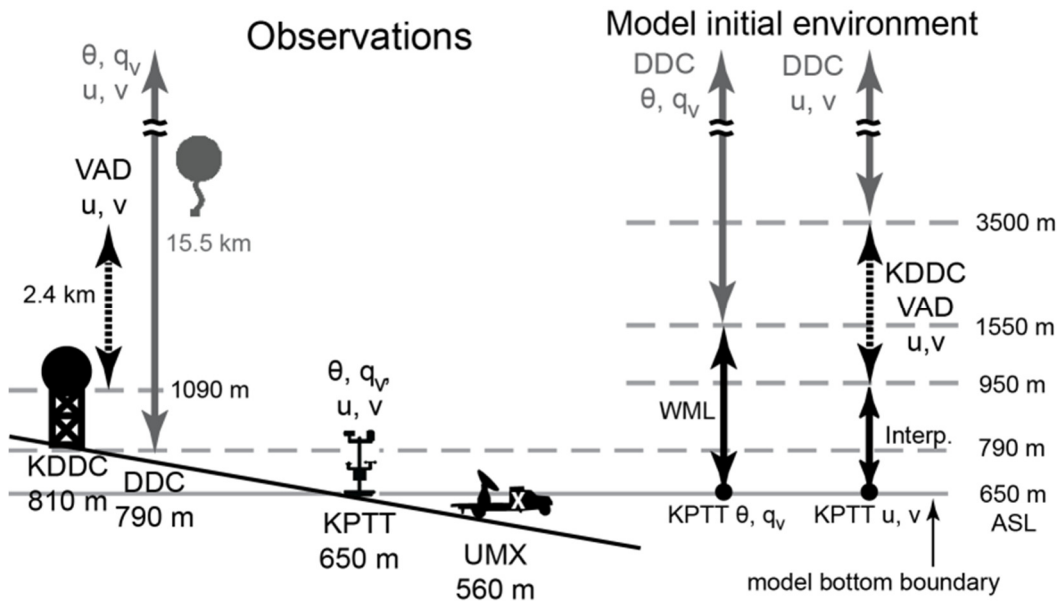
8

9

Fig. 3. Side-by-side comparisons of (a, b) Z and (c, d)  $V_r$  data collected at 0230 UTC (when tornado 5 was mature) by (a, c) KDDC at  $0.5^\circ$  and (b, d) UMass X-Pol at  $2.9^\circ$ . All panels use the same scale and are centered on the vortex. Range rings are every 15 km. UMass X-Pol reflectivity was attenuated on the north side of the Greensburg storm because of large hail in the storm core;  $V_r$  data in this region were manually excluded.  $V_r$  data were manually dealiased. UMass X-Pol  $V_r$  data were further edited to exclude “noisy” velocity data outside the storm, but some gates close to the radar, which contain information about the near-surface wind fields, were retained.

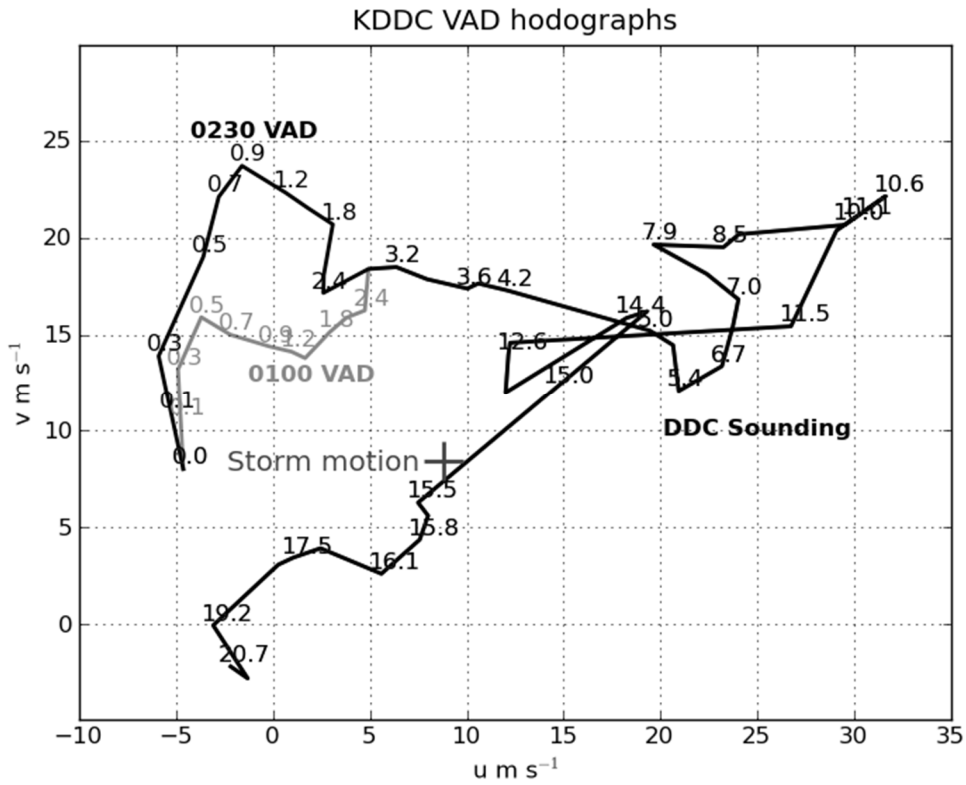
10

1  
2



3  
4  
5

Fig. 4. Observations used in the construction of the model initial environment. Heights and distances between observing platforms are not to scale.



1

2

3

4

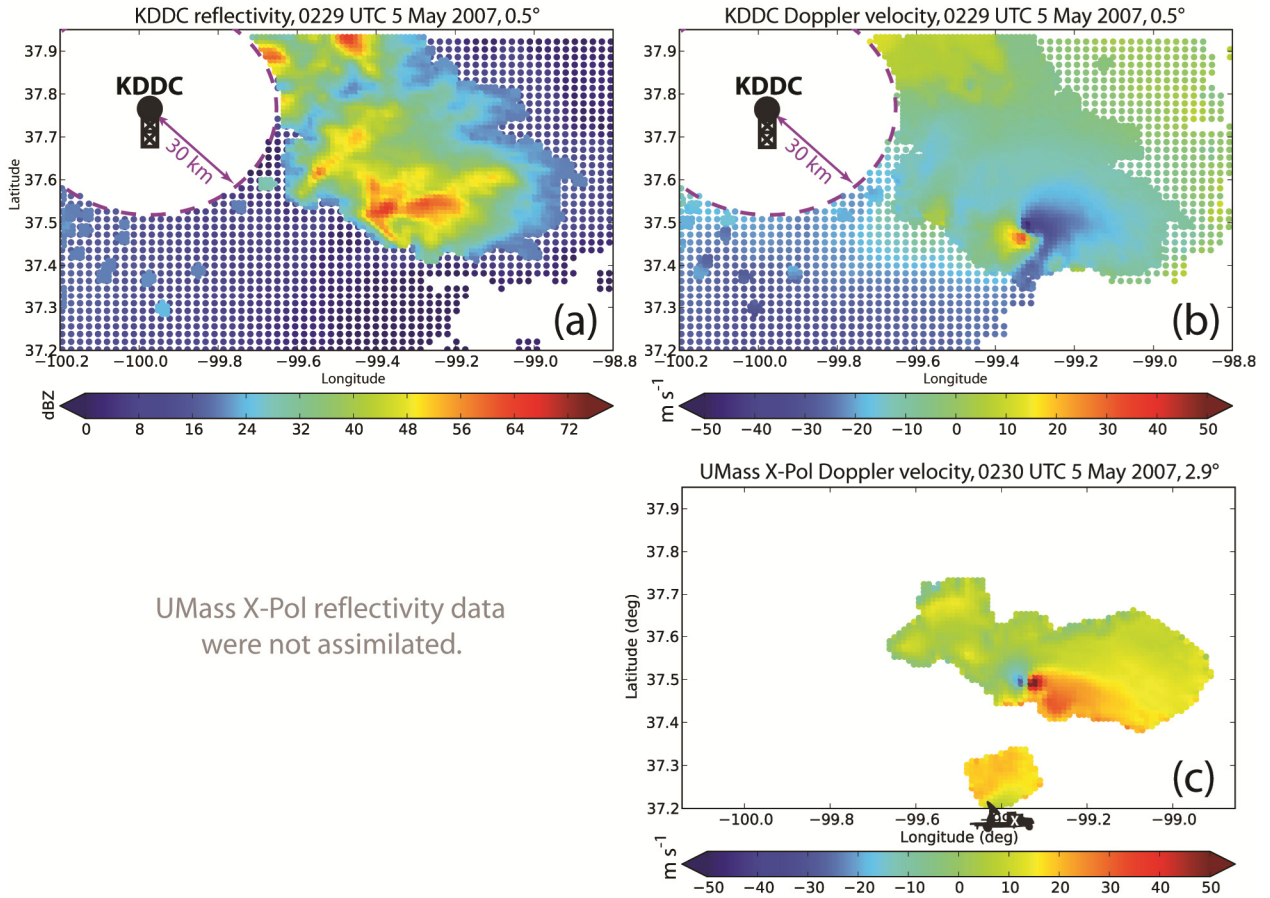
5

6

7

8

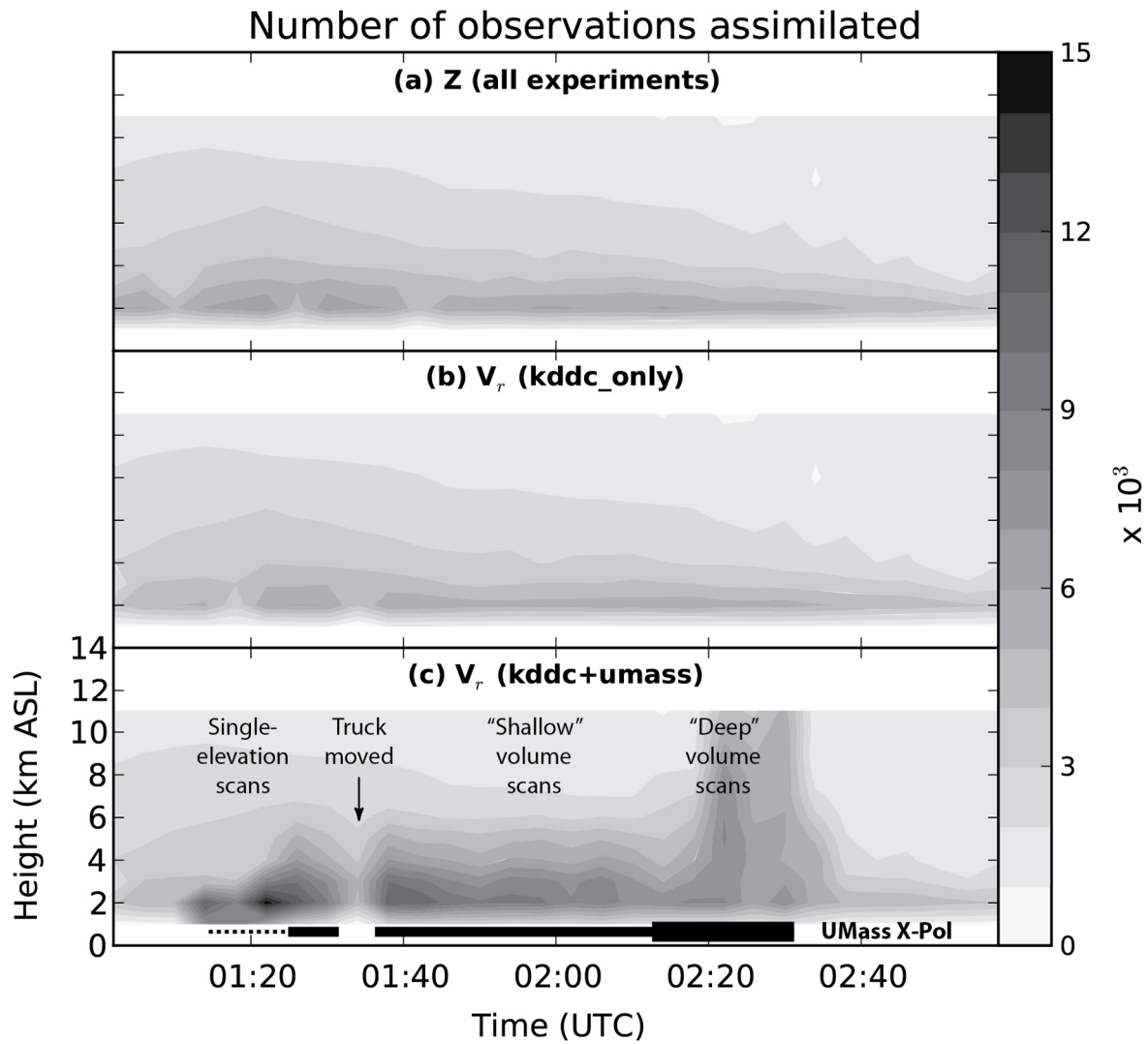
Fig. 5. Hodographs of the initial wind profiles used in the EnKF experiments prior to interpolation to the model grid levels. The black (gray) curve depicts the “vad0230” (“vad0100”) wind profile. Greensburg storm motion is denoted by a dark gray cross. Altitude labels are in km AGL. The surface velocity components are from the KPTT observation at 0210 UTC on 5 May 2007, while those in the 0.3 – 3.0 km layer are from KDDC VAD retrievals. The wind profiles above 3.0 km are from the 5 May 2007, 0000 UTC DDC sounding and are identical for both experiments.



1  
2  
3  
4  
5  
6  
7  
8  
9

Fig. 6. Objectively analyzed KDDC (a) reflectivity (in dBZ) and (b) Doppler velocity (in  $m s^{-1}$ ) collected at 0229 UTC at an elevation angle of  $0.5^\circ$ , and (c) objectively analyzed UMass X-Pol Doppler velocity (in  $m s^{-1}$ ) collected at 0230 UTC at an elevation angle of  $2.9^\circ$ . KDDC observations associated with reflectivity values greater than or equal to (less than) 20 dBZ were analyzed at 1 km (2 km) grid spacing. The dashed purple circle denotes the 30 km range ring around KDDC; data inside this radius were discarded for the lowest three elevation angles ( $0.5^\circ$ ,  $0.9^\circ$ , and  $1.3^\circ$ ) in each volume in order to avoid ground clutter targets.

1



2

3

4

5

6

7

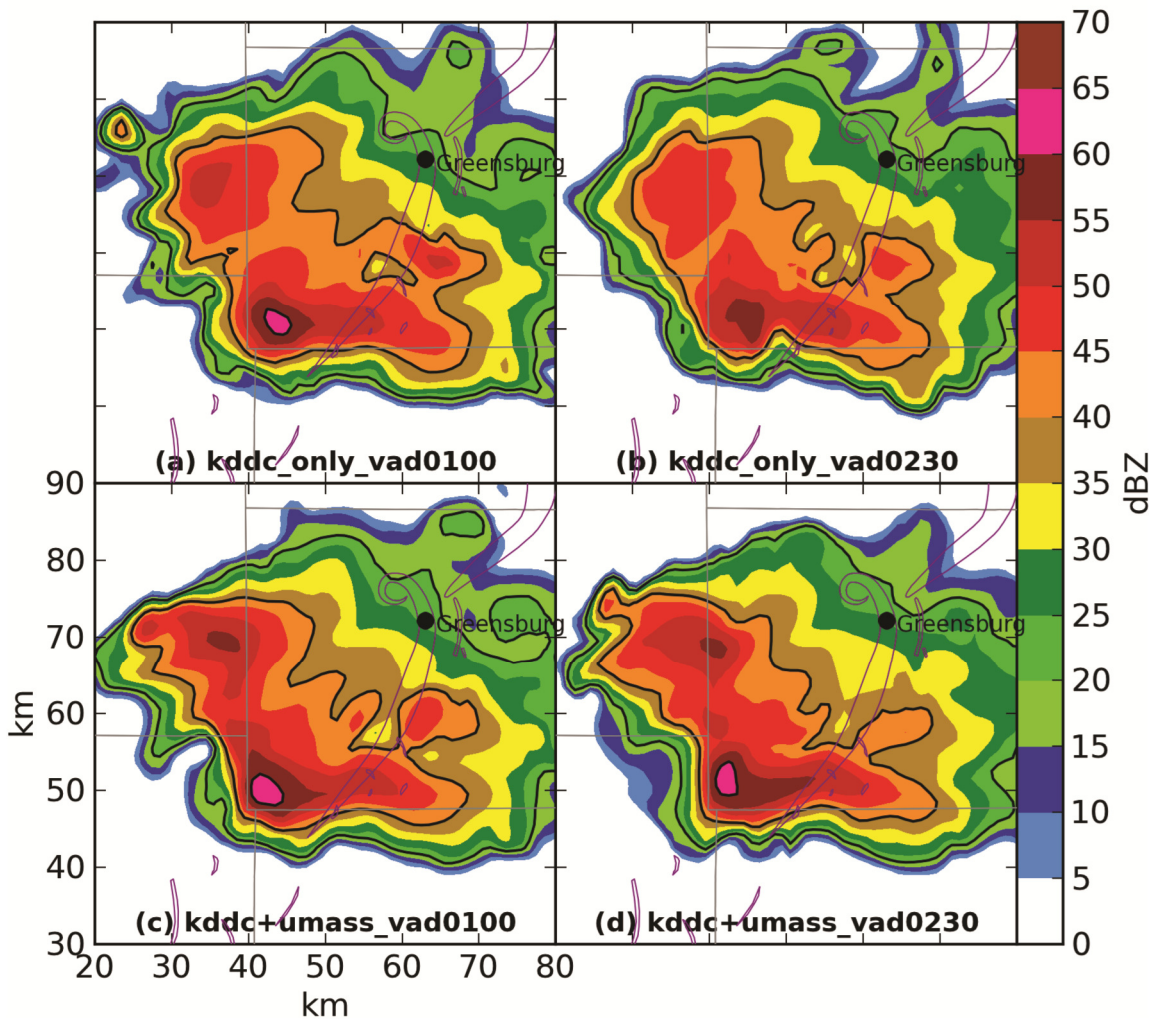
8

9

Fig. 7. Number of (a)  $Z$  and (b, c)  $V_r$  observations (e.g., Fig. 6) available for assimilation as a function of time and altitude. UMass X-Pol  $Z$  observations are not shown because they were not assimilated; the  $Z$  observations are only from KDDC and are the same for all experiments. Times when UMass X-Pol collected shallow and deep volumes (Fig. 2) are delineated in panel (c). Observations are plotted in 4-minute bins for clarity. The movement out of the domain of the Greensburg storm (as well as other storms) explains the overall decrease with time of both KDDC  $Z$  and  $V_r$  observations.

10

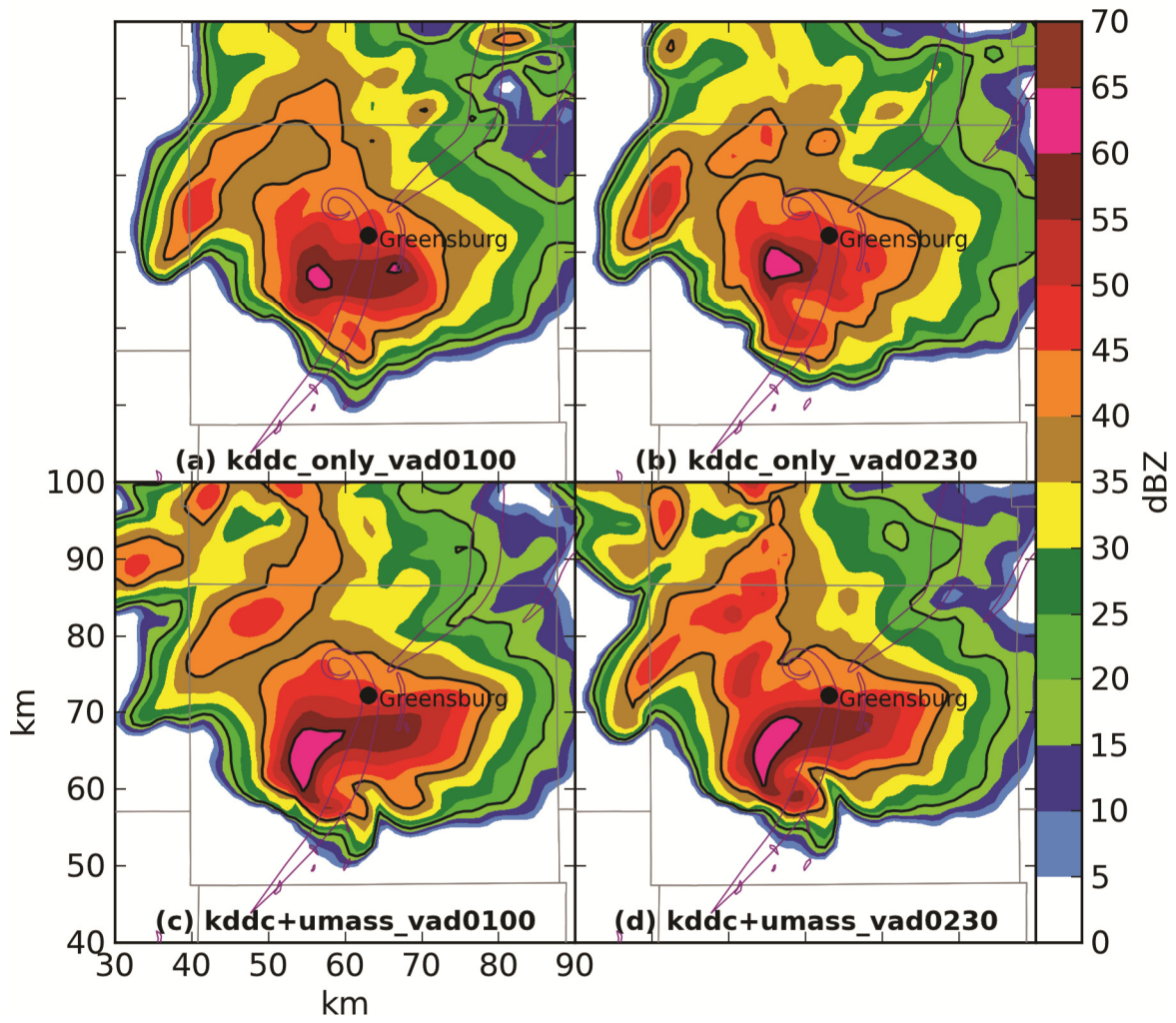
Ens. Mean Reflectivity, 05 May 2007 02:00:00, 750 m AGL



1  
2  
3  
4  
5  
6

Fig. 8. Prior ensemble mean reflectivity (in dBZ) at 0.8 km AGL at 0200 UTC (when the Greensburg tornado formed) for experiments (a) kddc\_only\_vad0100, (b) kddc\_only\_vad0230, (c) kddc+umass\_vad0100, and (d) kddc+umass\_vad0230. County boundaries are drawn in gray; tornado damage tracks are outlined in purple.

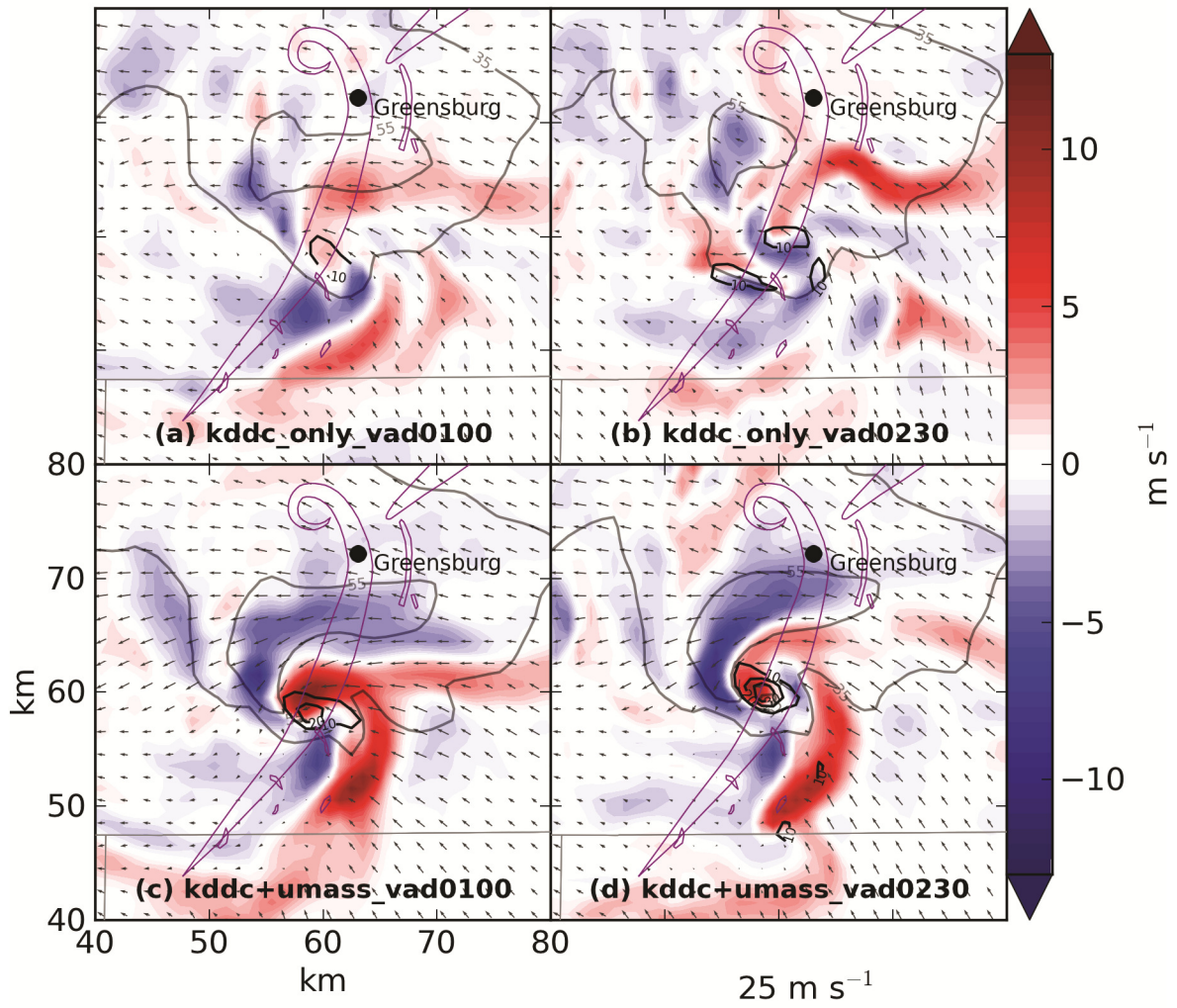
Ens. Mean Reflectivity, 05 May 2007 02:30:00, 750 m AGL



1  
2  
3

Fig. 9. As in Fig. 8, but at 0230 UTC (when the Greensburg tornado was mature).

Ens. Mean Vertical Velocity, 05 May 2007 02:30:00, 750 m AGL



1

2

3

4

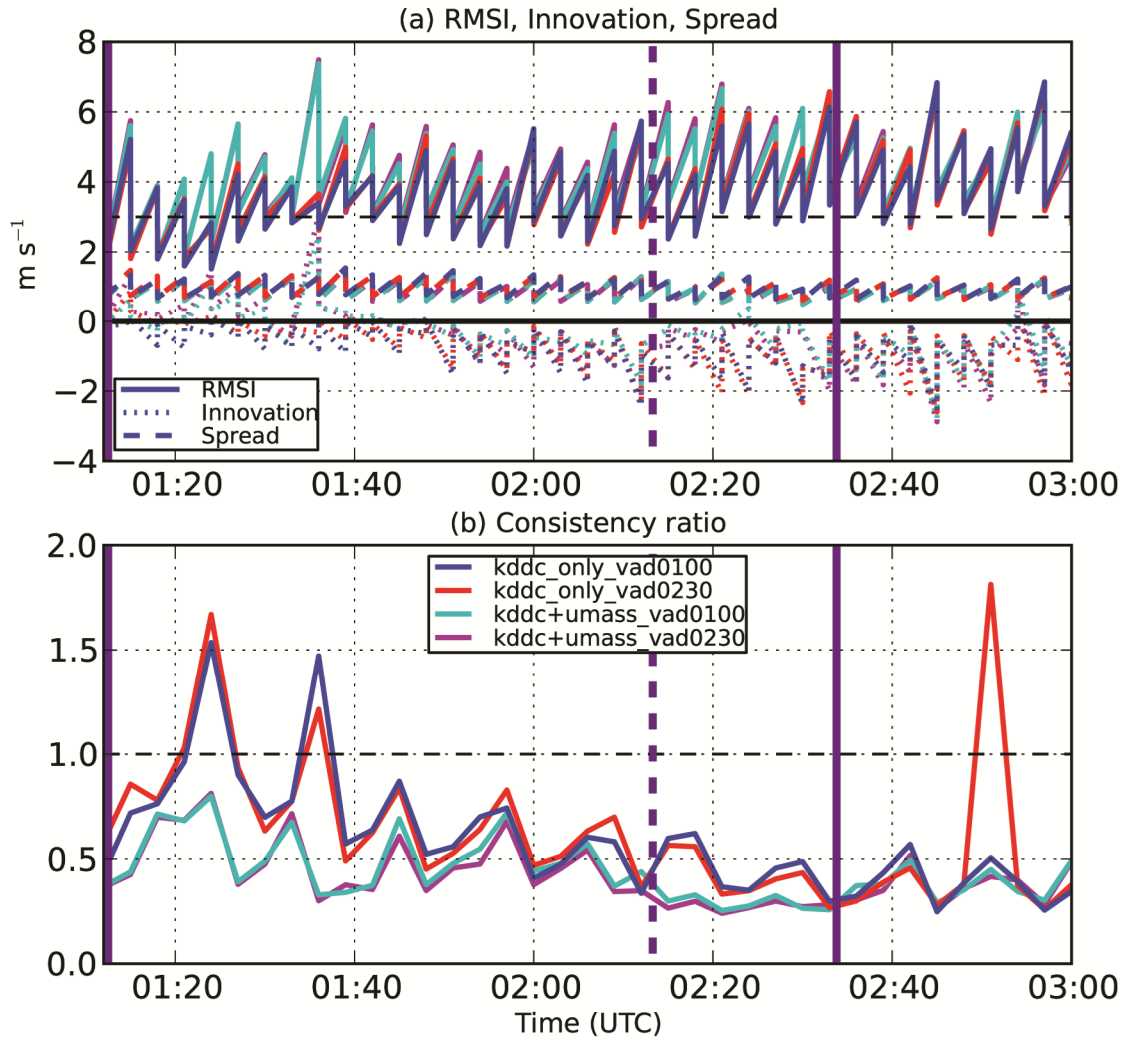
5

6

Fig. 10. As in Fig. 9, but slightly enlarged and showing prior ensemble mean vertical velocity (colored shading in  $\text{m s}^{-1}$ ), vorticity (solid black contours in  $10^{-3} \text{ s}^{-1}$ , starting from  $10 \times 10^{-3} \text{ s}^{-1}$ ), reflectivity (gray contours at 35 and 55 dBZ), and storm-relative velocity vectors (drawn every 2 km).

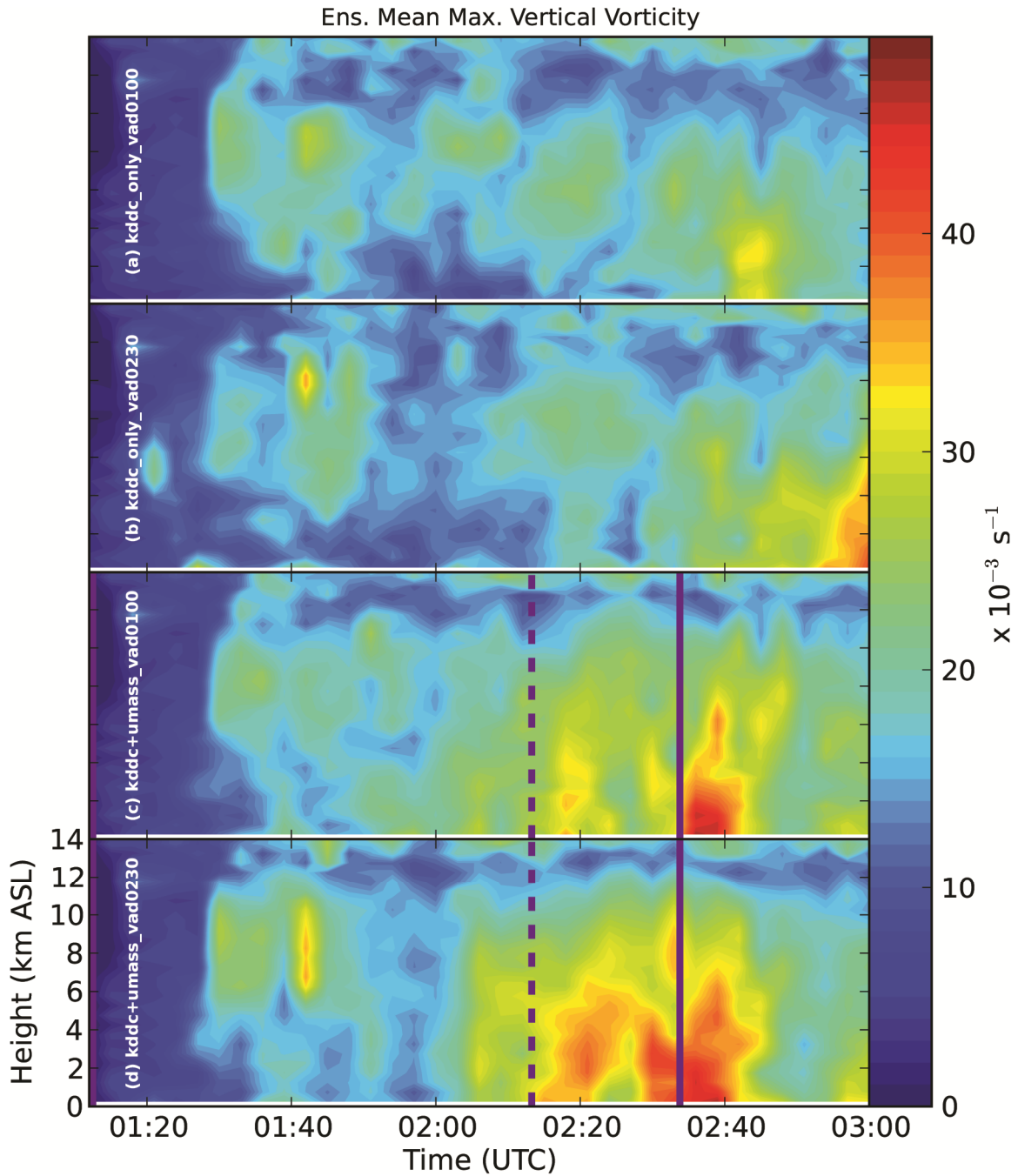


Doppler Velocity ( $V_r$ ), 0.0 - 12.0 km AGL



1  
2  
3  
4  
5  
6  
7

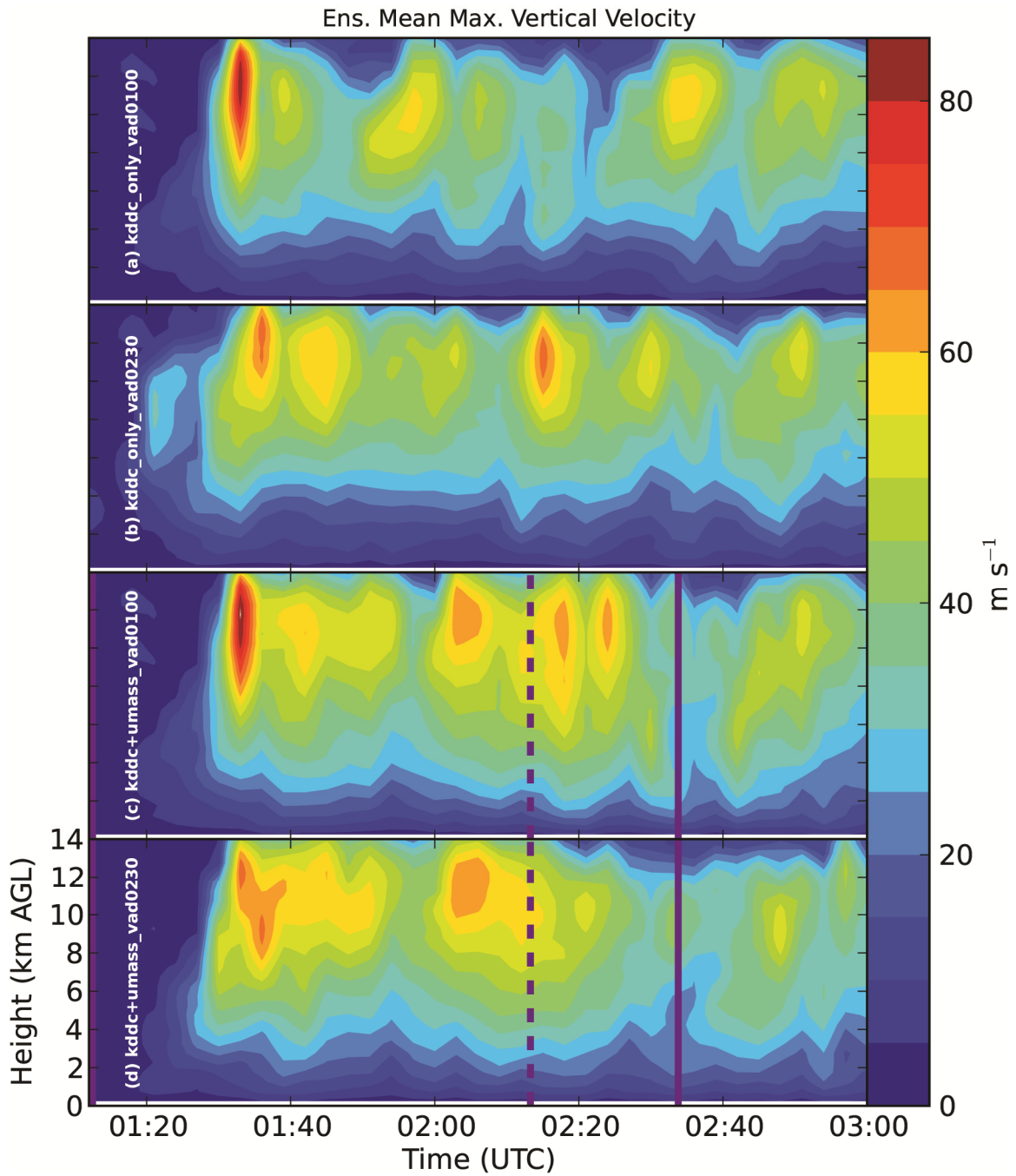
Fig. 12.  $V_r$  (a) RMSI (solid), mean innovation (dotted), and ensemble spread (dashed; in  $\text{m s}^{-1}$ ) and (b) consistency ratio (unitless). In panel (a), a horizontal dashed line marks  $\sigma_{v_r} = 3.0 \text{ m s}^{-1}$ . In panel (b), a horizontal dashed line marks unity. Vertical purple lines mark the start and end of UMass X-Pol volumetric data collection (Fig. 7); the dashed line marks when UMass X-Pol switched from collecting “shallow” to “deep” volumes.



1

2 Fig. 13. Time-height plot of prior ensemble mean maximum vertical vorticity (in  $10^{-3} \text{ s}^{-1}$ ) for  
 3 experiments (a) kddc\_only\_vad0100, (b) kddc\_only\_vad0230, (c) kddc+umass\_vad0100, and (d)  
 4 kddc+umass\_vad0230. Vertical purple lines mark changes in UMass X-Pol volumetric data  
 5 collection as in Fig. 12.

6



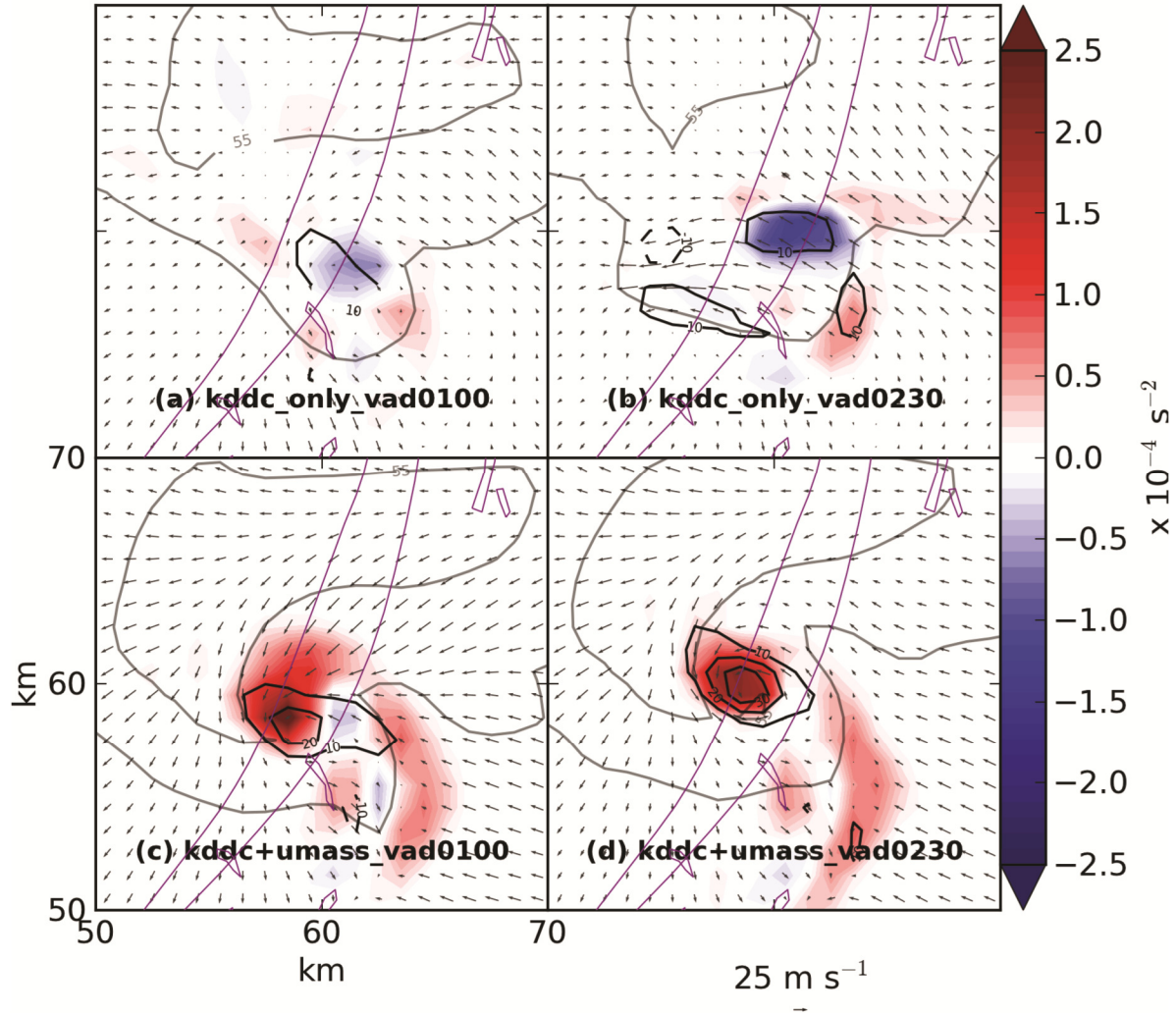
1

2

Fig. 14. As in Fig. 13, but for ensemble mean maximum vertical velocity (in  $\text{m s}^{-1}$ ).

3

Ens. Mean Stretching, 05 May 2007 02:30:00, 750 m AGL

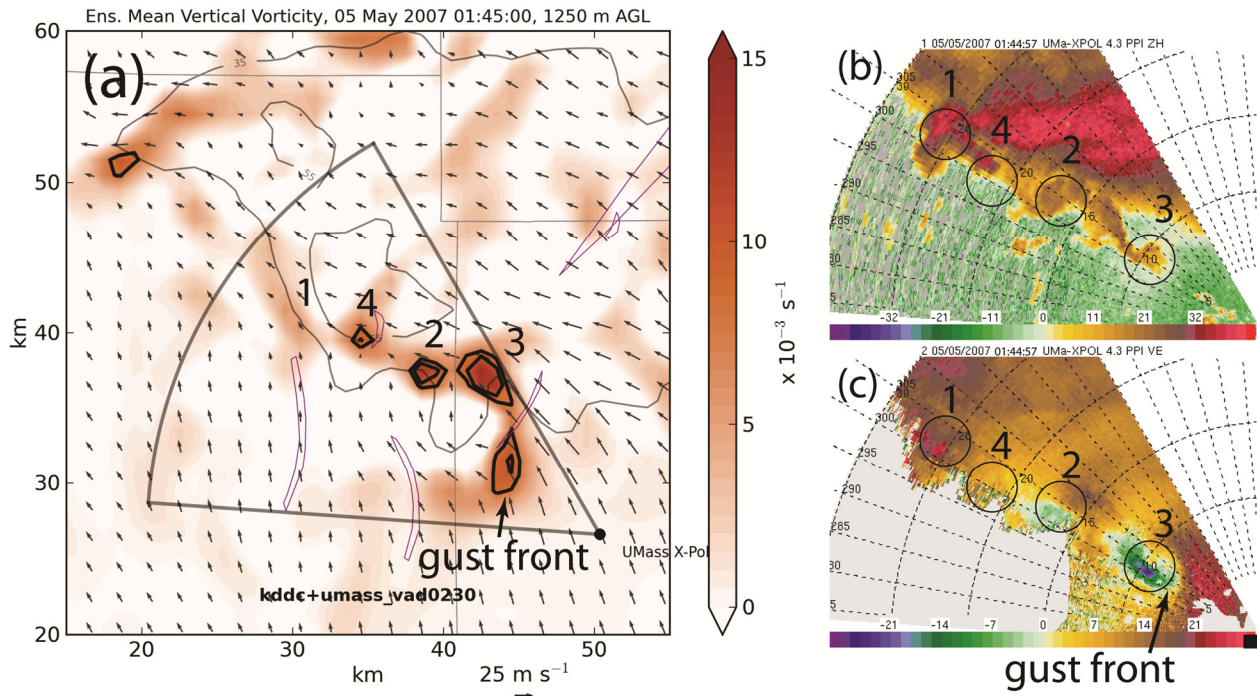


1

2 Fig. 15. As in Fig. 9, but showing the stretching term of the vertical vorticity tendency equation (in  $10^{-4} \text{ s}^{-2}$ ).  
3 Note that the panels are enlarged relative to those in Fig. 9, and that velocity vectors are drawn every 1 km.

4

1



2

3

4

5

6

7

8

9

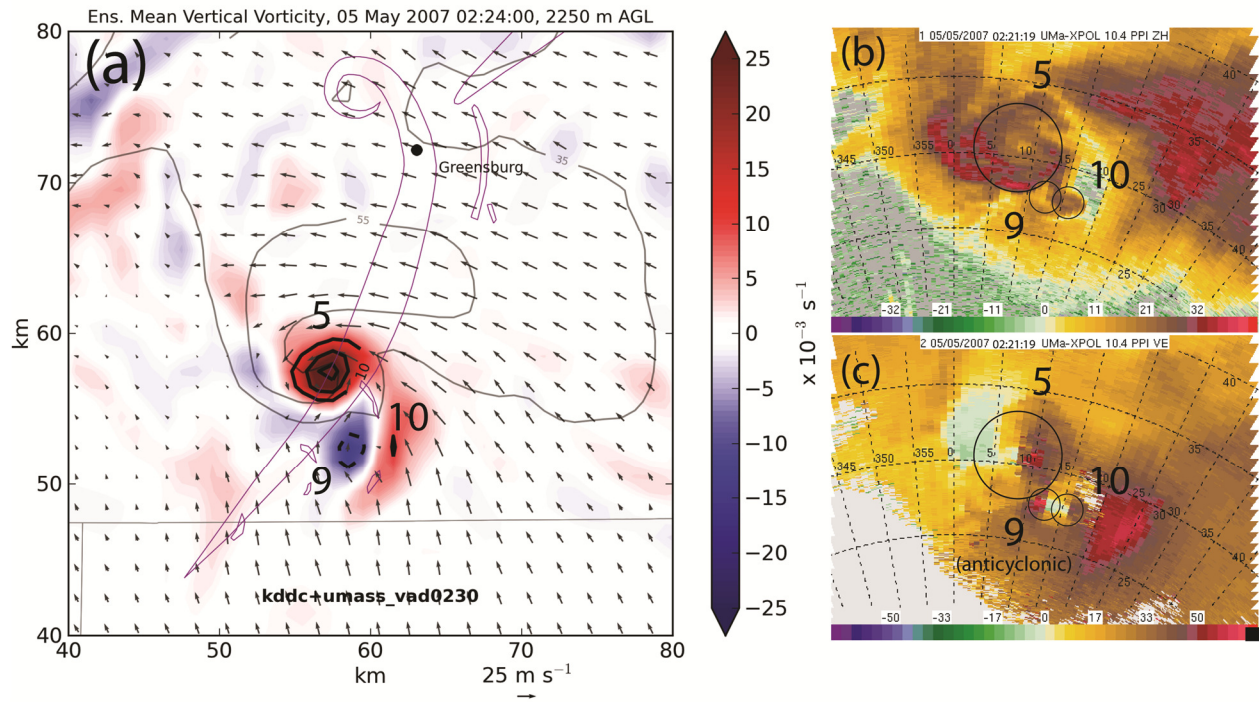
10

11

12

Fig. 16. (a) Ensemble mean analyzed vertical vorticity (colored shading), with solid black contours plotted at  $8 \times 10^{-3} \text{ s}^{-1}$  and  $10 \times 10^{-3} \text{ s}^{-1}$ , reflectivity (gray contours at 35 and 55 dBZ), and storm-relative velocity vectors (plotted at 2 km intervals) at 1.3 km AGL for the kddc+umass\_vad0230 experiment. Only positive values of vertical vorticity are plotted in panel (a), and the outline of the UMass X-Pol sector is overlaid. (b) UMass X-Pol uncalibrated reflectivity (in dBZ) and (c) Doppler velocity (in  $\text{m s}^{-1}$ ) at an elevation angle of  $4.3^\circ$ . Vertical vorticity maxima and circulations corresponding to tornadoes are circled and numbered as in Lemon and Umscheid (2008). At this time (0145 UTC), tornado 1 was dissipating, tornado 2 had already dissipated into a remnant vortex, tornado 3 was developing, and tornado 4's vortex was forming above the  $4.3^\circ$  elevation angle sweep surface.

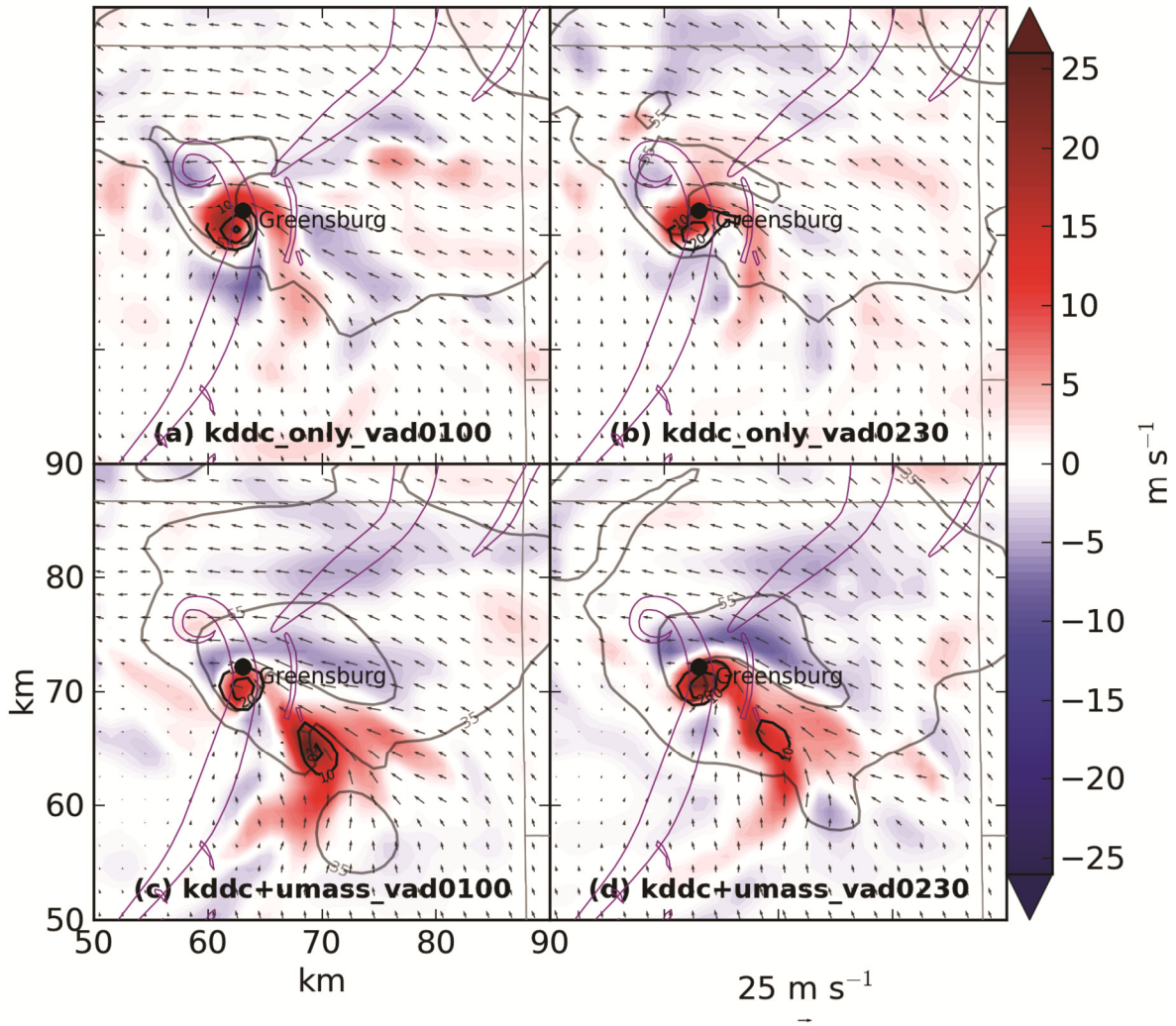
13



1  
2  
3  
4  
5  
6  
7  
8  
9

Fig. 17. (a) Ensemble mean analyzed vertical vorticity (colored shading) with solid black contours plotted at  $-10 \times 10^{-3} \text{ s}^{-1}$  (dashed) and at intervals of  $10 \times 10^{-3} \text{ s}^{-1}$  starting at  $10 \times 10^{-3} \text{ s}^{-1}$  (solid), reflectivity (gray contours at 35 and 55 dBZ), and storm-relative velocity vectors (plotted at 2 km intervals) at 2.3 km AGL at 0224 UTC for the `kddc+umass_vad0230` experiment. (b) UMass X-Pol uncalibrated reflectivity (in dBZ) and (c) Doppler velocity (in  $\text{m s}^{-1}$ ) at an elevation angle of  $10.4^\circ$  at 0221 UTC. Vertical vorticity maxima and circulations corresponding to tornadoes are circled and numbered as in Lemon and Umscheid (2008). Note that tornado 9 was anticyclonic.

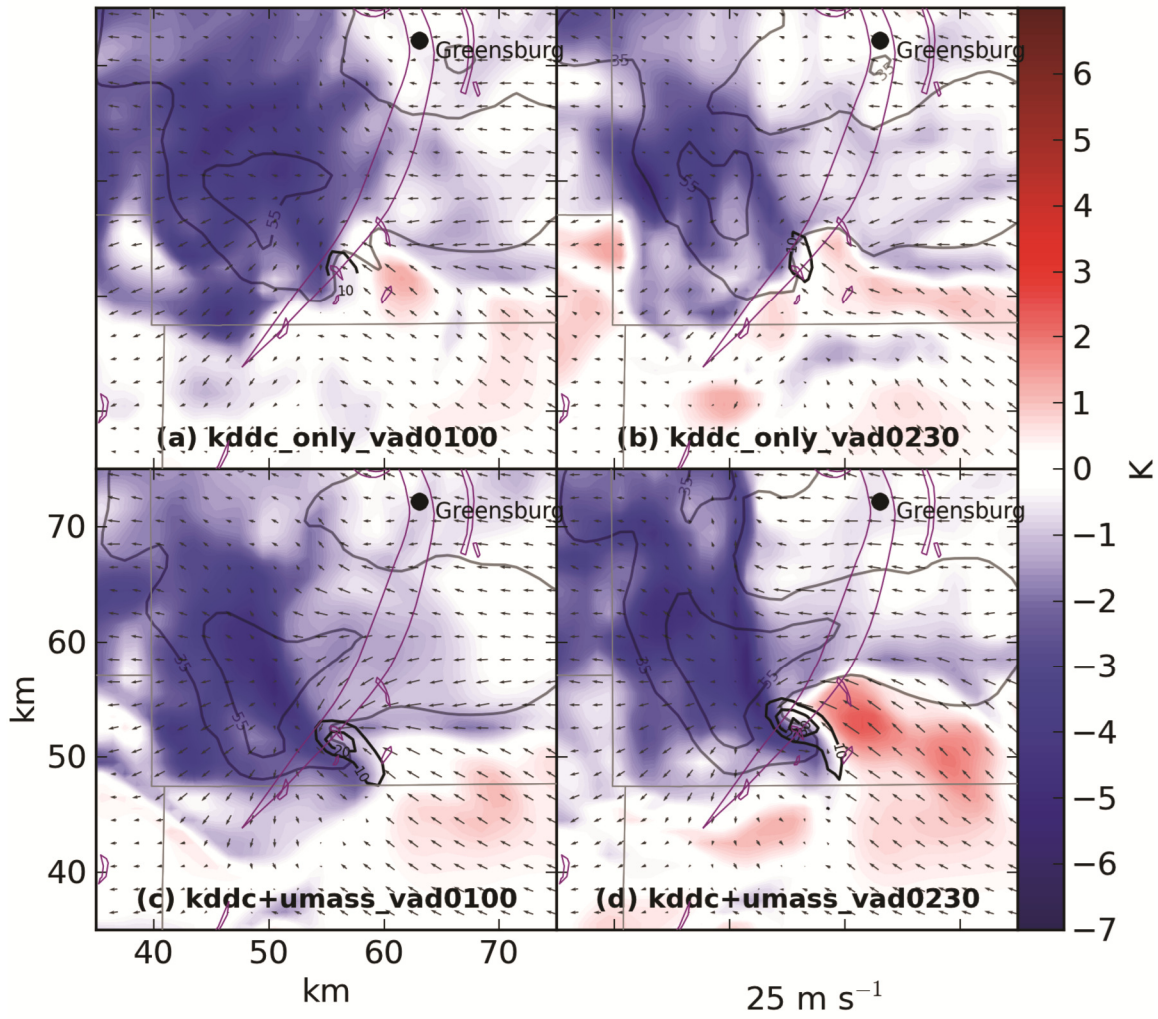
Ens. Mean Vertical Velocity, 05 May 2007 02:45:00, 2250 m AGL



1  
2  
3

Fig. 18. As in Fig. 10, but at 0245 UTC, 2.3 km AGL, and shifted slightly northeast.

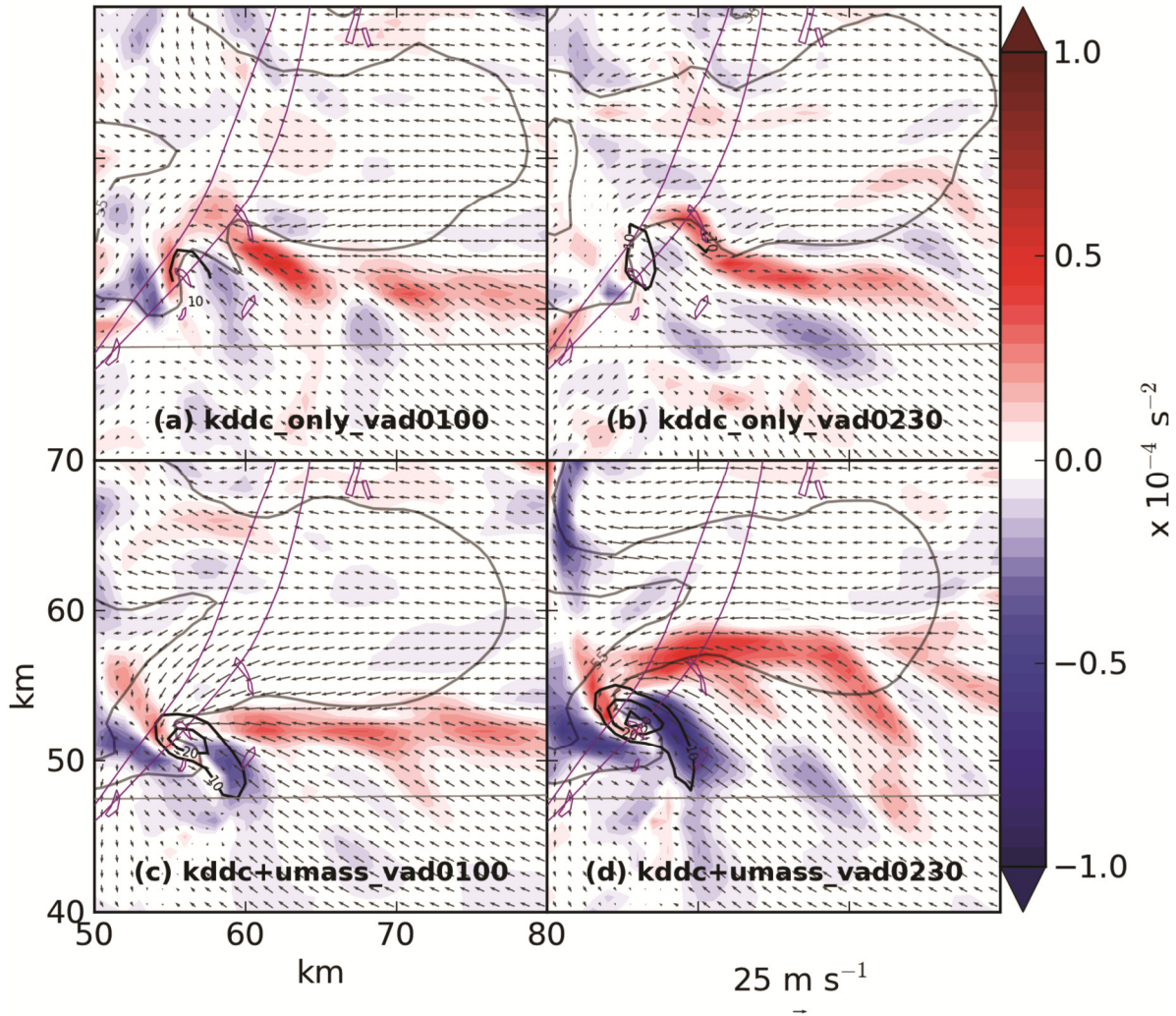
Ens. Mean Pert. Pot. Temp, 05 May 2007 02:15:00, 250 m AGL



1  
2  
3  
4  
5  
6  
7

Fig. 19. Ensemble mean perturbation potential temperature (color shading, in K) at 0.3 km AGL (the model level closest to the surface), vertical vorticity (solid black contours) at intervals of  $10 \times 10^{-3} \text{ s}^{-1}$  starting at  $10 \times 10^{-3} \text{ s}^{-1}$ , reflectivity (gray contours at 35 and 55 dBZ), and storm-relative velocity vectors (plotted at 2 km intervals) at 0215 UTC. Potential temperatures are plotted relative to the initial model state ( $\theta=306.7 \text{ K}$ ).

Ens. Mean Streamwise Baroclinic Gen., 05 May 2007 02:15:00, 750 m AGL



1

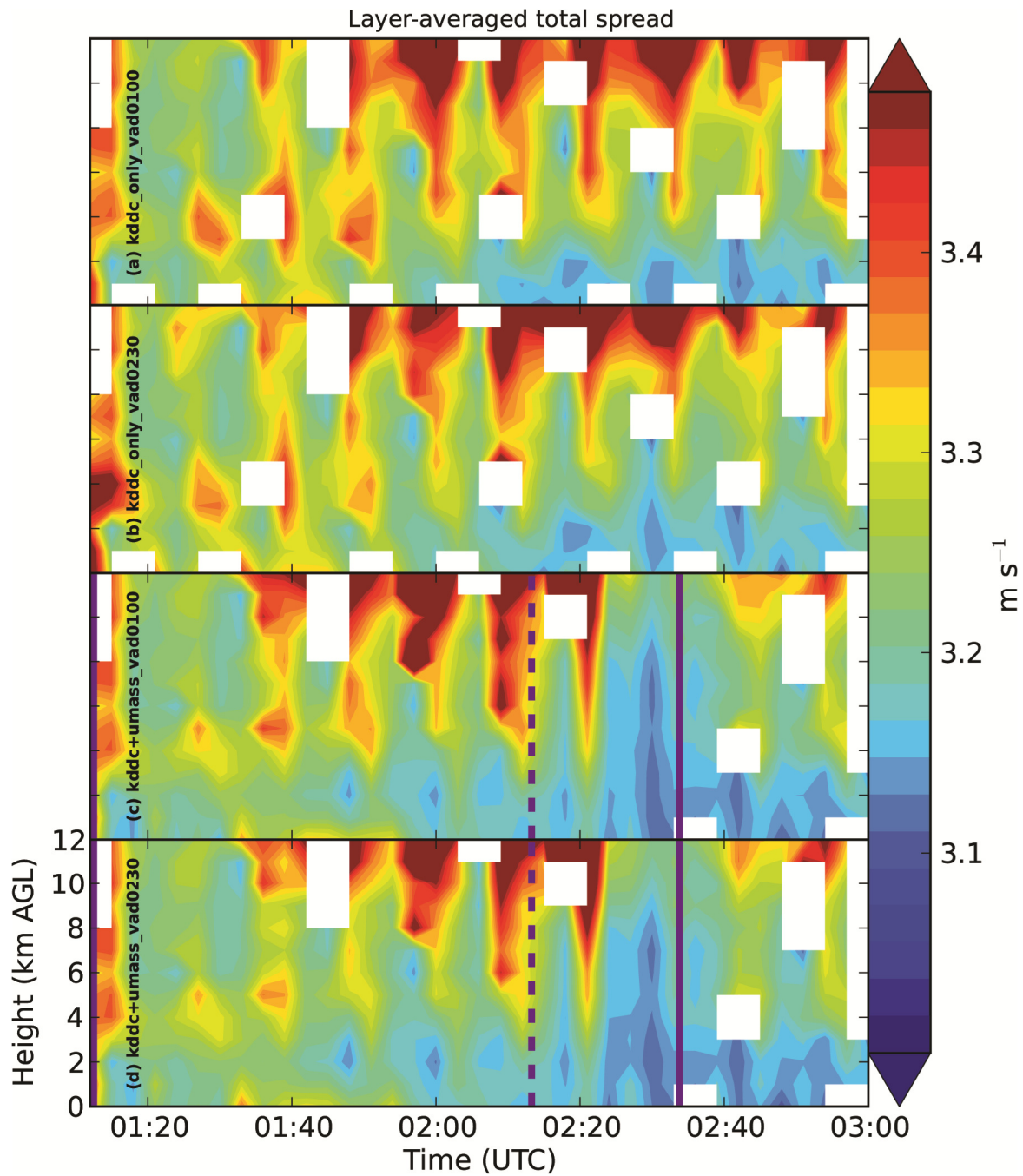
2

3

4

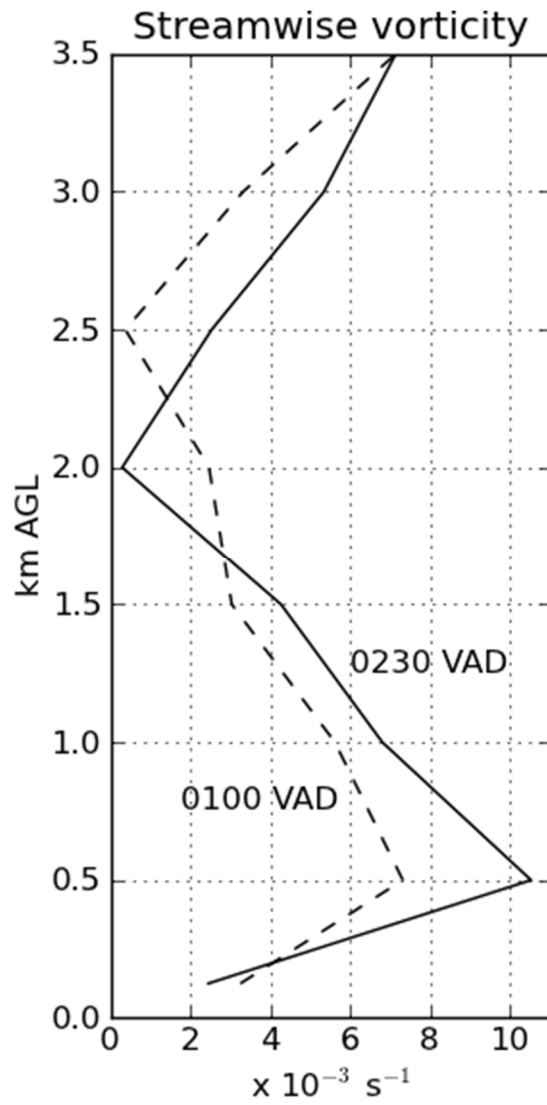
5

Fig. 20. As in Fig. 15, but showing the ensemble mean baroclinic generation of storm-relative streamwise horizontal vorticity (in  $10^{-4} \text{ s}^{-2}$ ) at 0215 UTC. Note that the panels are compressed and shifted relative to those in Fig. 15.



1

2 Fig. 21. Layer-averaged total spread (in  $\text{m s}^{-1}$ ) over the entire domain for experiments (a)  
 3 kddc\_only\_vad0100, (b) kddc\_only\_vad0230, (c) kddc+umass\_vad0100, and (d)  
 4 kddc+umass\_vad0230. Vertical purple lines mark changes in UMass X-Pol volumetric data  
 5 collection as in Fig. 12. White rectangles denote regions where statistically insignificant number  
 6 of observations were assimilated.



1

2

3

4

Fig. 22. Vertical profiles of storm-relative streamwise horizontal vorticity associated with the hodographs depicted in Fig. 5.